L.B.Krivdin
Russ. Chem. Rev., 2020, **89** (4) 449 – 468

https://doi.org/10.1070/RCR4927

Computational liquid-phase and solid-state ^{29}Si NMR

Leonid B. Krivdin [a, b]

[a] *A.E.Favorsky Irkutsk Institute of Chemistry, Siberian Branch of the Russian Academy of Sciences, ul. Favorskogo 1, 664033 Irkutsk, Russian Federation*
[b] *Angarsk State Technical University, ul. Tchaikovskogo 60, 665835, Angarsk, Irkutsk Region, Russian Federation*

This review focuses on the computational aspects of ^{29}Si NMR chemical shifts and spin – spin coupling constants involving the ^{29}Si nucleus. It concentrates on the electronic and stereochemical effects manifesting in these parameters, calculated at different levels of theory with a special emphasis on their practical applications. For ^{29}Si NMR chemical shifts, a good deal of interest is focused on the less common solid state studies, in addition to more popular liquid state data. For spin – spin coupling constants, the main interest is concentrated on the mostly common ^{29}Si – ^{1}H and ^{29}Si – ^{13}C couplings. The review is written in memory of the Full Member of the Russian Academy of Sciences, Professor Mikhail G. Voronkov in view of his invaluable contribution to the field of organosilicon chemistry and ^{29}Si NMR.
The bibliography includes 93 references.

Contents

1. Introduction 450
2. Computation of ^{29}Si NMR chemical shifts 451
   2.1. Liquid phase 451
      2.1.1. Non-relativistic calculations 451
      2.1.2. Relativistic effects 453
   2.2. Solid state 456
3. Computation of spin – spin coupling constants involving the ^{29}Si nucleus 457
   3.1. Spin – spin coupling constants ^{29}Si – ^{1}H 457
   3.2. Spin – spin coupling constants ^{29}Si – ^{13}C 464
   3.3. Other coupling constants ^{29}Si – X 465
4. Conclusion 466

In memory of Academician Mikhail Grigorievich Voronkov, to commemorate his achievements in the Chemistry of Silicon and ^{29}Si NMR



Academician Mikhail Voronkov (1921 – 2014)

This photo was taken by the author in 2007 during the Annual Scientific Session of A.E.Favorsky Irkutsk Institute of Chemistry.

Mikhail Voronkov graduated from the Leningrad State University in 1942 and received his PhD in 1947 and DSc in 1954. He became the Head of the Laboratory of Inorganic Polymers at the Institute of Chemistry of Silicates, USSR Academy of Sciences (1954 – 1991) and the Head of the Laboratory of Organoelement Compounds at the Institute of Organic Synthesis, Latvian Academy of Sciences (1961 – 1970). He was elected the Corresponding Member of the Academy of Sciences of Latvian SSR in 1966 and the Corresponding Member of the USSR Academy of Sciences in 1970. He was the Director of Irkutsk Institute of Organic Chemistry, Siberian Branch of the USSR Academy of Sciences for a quarter of a century, from 1970 to 1994. In 1995 he became a Scientific Adviser of the Russian Academy of Sciences and a Head of the Laboratory of the Organoelement Compounds at the same institute. In 1992, in recognition of his distinguished service to chemistry, he received the title of the Academician of the USSR Academy of Sciences.

Leonid Krivdin graduated from M.V.Lomonosov Moscow State University in 1977, received his PhD in 1982 from the Irkutsk State University which was followed by a post-doctoral fellowship at Flinders University of South Australia in the group of Professor Ernst Della (1990 – 1991). He received his DSc in 1989, and Full Professor in 1993.
His research interests focus on computation of NMR parameters being substantiated with some 400 research publications including 10 reviews and book chapters. Under his scientific supervision, 11 PhD and 1 DSc dissertations were defended in the interim of 1989 till present. He is currently a Chief of NMR Laboratory at A.E.Favorsky Irkutsk Institute of Chemistry and a Chair of Chemistry at Angarsk State Technical University.
E-mail: krivdin_office@irioch.irk.ru

Received 25 October 2019

© 2020 Uspekhi Khimii, ZIOC RAS, Russian Academy of Sciences and IOP Publishing Limited

He published some 3500 scientific papers and 55 books and book chapters and supervised 35 DSc and about 150 PhD dissertations.

For more than 50 years of his scientific activity in the field of organosilicon chemistry and ^{29}Si NMR, M.G.Voronkov has been a prominent scientist and one of the most cited chemists in the world literature. He has discovered a number of novel reactions and classes of organosilicon compounds and introduced a wide variety of organosilicon reagents including trimethyliodosilane, bis(trimethylsiloxy)phosphine, bis(trimethylsilyl) sulfate, organyltrifluorosilanes, and trimethylsilyl nitrate. He is considered to be the founder of a new branch of silicon chemistry, namely bioorganosilicon chemistry. During the last years of his scientific activity he performed the pioneering investigation of biologically active compounds together with their use in medicine and agriculture. He created some novel chemical reagents for different applications in agriculture, including stimulants of reproductive activity of animals and plants, growth-regulating agents, and adaptogens, increasing the stability of living organisms to extreme conditions of their life and environment.

Academician Voronkov made a great contribution to the development of theoretical, synthetic and applied organosilicon chemistry, dealing, in particular, with hypervalent silicon compounds, especially those which he named silatranes and dragonoids. His most fundamental studies were directed to the chemistry of unusual three-, penta- and hexacoordinated silicon compounds, bioactive organosilicon compounds, new carbofunctional organosilicon monomers and polymers, heteroatomic organosilicon compounds (heterosiloxanes), polyunsaturated macrocyclic silicohydrocarbons, and heteroorganic silicon compounds involving boron, aluminium, tin, titanium, phosphorus, arsenic, antimony, selenium, and tellurium.

His invaluable contributions to organotin chemistry included the studies of compounds containing tin-sulfur bonds, hypervalent tin, homolytic addition reactions to alkenylstannanes, and the application of organotin compounds in organic synthesis. M.G.Voronkov introduced a new generation of unique hemostatics based on polymetal acrylates providing an effective antimicrobial action, as well as wound, burn healing and antitumour action. A series of unique drugs such as feracryl, argakril, acyzolum, trecrezan, silacast, silimin, dibutyrin, and cobazol, together with the original adaptogens, immunomodulators and antidotes, were developed under his guidance and supervision. Many of these research projects were carried out in collaboration with the leading universities of Asia, Europe and the United States.

In recognition of his scientific achievements, M.G. Voronkov received an Honorary Doctorate from Polytechnika Gdanska (Poland). He was elected Corresponding Member of the Braunschweig Scientific Society (Germany) and of the Chemical Society of Japan. He was also elected a Foreign Member of the Latvian Academy of Sciences and a Member of the Union of Latvian Chemists. He was elected a Member of the Asia-Pacific Academy of Materials, an honorary Member of Florida Center of Heterocyclic Chemistry (USA), and an honorary Professor of Ulan-Bator University (Mongolia). He was a Member of the Advisory Board and an active participant at the Nobel Symposium Biochemistry of silicon and related problems (Sweden) and a Member of the Organizing Committee and a plenary lecturer at almost all International Symposia on Organosilicon Chemistry. Also, M.G. Voronkov was a Member of the Editorial Boards of four international journals: Journal of Organometallic Chemistry, Chemistry of Heterocyclic Compounds, ARKIVOC, and Russian Journal of General Chemistry. For his distinguished achievements in organosilicon chemistry, M.G.Voronkov was awarded the State Prize of Ukraine and the State Prize of the Russian Federation.

1. Introduction

Theoretical aspects of the calculation of NMR parameters are thoroughly reviewed in a fundamental handbook of molecular electromagnetism by Stephan Sauer[1] and in a number of related reviews on theoretical and computational aspects of NMR parameters.[2–18] Papers, dealing with theoretical calculations of ^{29}Si NMR chemical shifts and spin–spin coupling constants, are much less common than those, dealing with the calculation of proton,[19–21] carbon,[22–24] nitrogen,[25] and phosphorus[26,27] NMR parameters. However, the former do exist in a sufficient number, and, based on those publications, in the present review we tried to trace out and to systemize the general trends in this field. The first part of the review deals with the computation and structural application of calculated ^{31}Si NMR chemical shifts in liquid phase and solid state, while the second part focuses on the computational aspects of spin–spin coupling constants involving silicon (mainly, ^{29}Si–^{1}H and ^{29}Si–^{13}C couplings) in particular classes of organosilicon compounds. The review, as a whole, is oriented toward NMR spectroscopists and a broad audience of researchers, working with organosilicon compounds and utilizing modern computational methods in their everyday lives for the calculation and interpretation of experimental ^{29}Si NMR spectra.

Glossary of abbreviations and symbols:

BO — bridging oxygen atom,

CBS — complete basis set,

CCSD — coupled cluster single and double excitation model,

CCSD(T) — coupled cluster single and double excitation model with perturbative triples corrections;

DFT — density functional theory,

DFTB — density-functional based tight-binding,

GIAO — Gauge invariant atomic orbital,

HALA — heavy atom on light atom (effect),

HF — Hartree–Fock,

HOMO — highest occupied molecular orbital,

IEF-PCM— integral equation formalism polarizable continuum model,

LDBS — locally dense basis set,

LUMO — lowest unoccupied molecular orbital,

MAE — mean absolute error,

MAPE — mean absolute percentage error,

MAS — magic angle spinning,

MO — molecular orbital,

MP2 — second-order Møller–Plesset perturbation theory,

NBdO — non-bridging oxygen atom,

NBO — natural bond orbitals,

NJC — natural J-coupling,

NMR — nuclear magnetic resonance,

PBE — Perdew–Burke–Ernzerhof (functional),

RHF — restricted Hartree–Fock,

RMS — root mean square,

RPA — random phase approximation,

SO — spin–orbit,

SOPPA — second-order polarization propagator approach,

SOPPA(MP2) — second-order polarization propagator approach in combination with Møller – Plesset perturbation theory,

SOPPA(CC2) — second-order polarization propagator approach in combination with second-order approximate coupled cluster model,

SOPPA(CCSD) — second-order polarization propagator approach in combination with coupled cluster single and double excitation model,

SSM — supermolecular solvation model,

TBO — three bridging oxygen atom,

ZORA — zeroth order regular approximation,

ZPVC — zero-point vibrational correction,

UP— uncontracted basis sets of partridge,

J — spin – spin coupling constant,

σ — shielding constant,

φ — dihedral angle,

δ_{iso} — isotropic chemical shift,

$\Delta\delta_{rel}$ — relativistic correction to chemical shift,

$\Delta\delta_{solv}$ — solvent correction to chemical shift,

$\Delta\sigma_{rel}$ — relativistic correction to shielding constant.

2. Computation of ^{29}Si NMR chemical shifts

2.1. Liquid phase

Calculations of ^{29}Si NMR chemical shifts in liquid phase for silanes containing no 'heavy' elements (*i.e.* those beginning with the 4-th period) can safely be performed at the non-relativistic level since the contribution of 'neat' relativistic effects of silicon is next to negligible. However, the situation dramatically changes when 'heavy' elements starting from the fourth period neighbouring to silicon are present in the molecule. In this case, relativistic calculations at the two- or four-component levels are strictly recommended.

2.1.1. Non-relativistic calculations

The 'new history' of the non-relativistic computational ^{29}Si NMR in liquid phase begins early this century (herewith, we do not go deeper in time) and may be illustrated with a paper by Milbradt *et al.*,[28] where the ^{29}Si NMR shielding constants and chemical shifts were calculated for a series of silicon compounds, silanes Si_nH_{2n+2} ($n = 1-5$), methylsilanes $H_nSi(CH_3)_{4-n}$, and phenylsilanes, $H_nSi(C_6H_5)_{4-n}$ ($n = 1-3$), using the so-called Density-Functional based Tight-Binding (DFTB) approach, as compared to the parent Density Functional Theory (DFT) method and experiment. Calculated in that way chemical shifts correlated quite well with their experimental values. After an empirical correction, ^{29}Si NMR chemical shifts for silanes and methylsilanes obtained within the DFTB scheme were equivalent to those obtained using pure DFT calculations. The RMS error with respect to experiment was 4.3 ppm in the range of *ca.* 80 ppm for silanes, and approximately the same for methylsilanes and phenylsilanes.

Much later, Anafcheh and Ghafouri[29] performed systematic DFT calculations of ^{29}Si NMR chemical shifts using B3LYP functional and Pople's 6-311G(d,p) basis set for a number of fluorinated polysilanes, Si_nF_n, with n ranging from 4 to 60, exemplified in Fig. 1. It was found that silicon chemical shifts indicated an equivalent electronic environment for silicon atoms within each of the considered smaller polysilane cages with $n = 20$ and less. However, a few additional peaks were present in the ^{29}Si NMR spectra of fluorinated silicon fullerenes with n of more than 20, as illustrated in Fig. 2. The Highest Occupied Molecular Orbital (HOMO) and Lowest Unoccupied

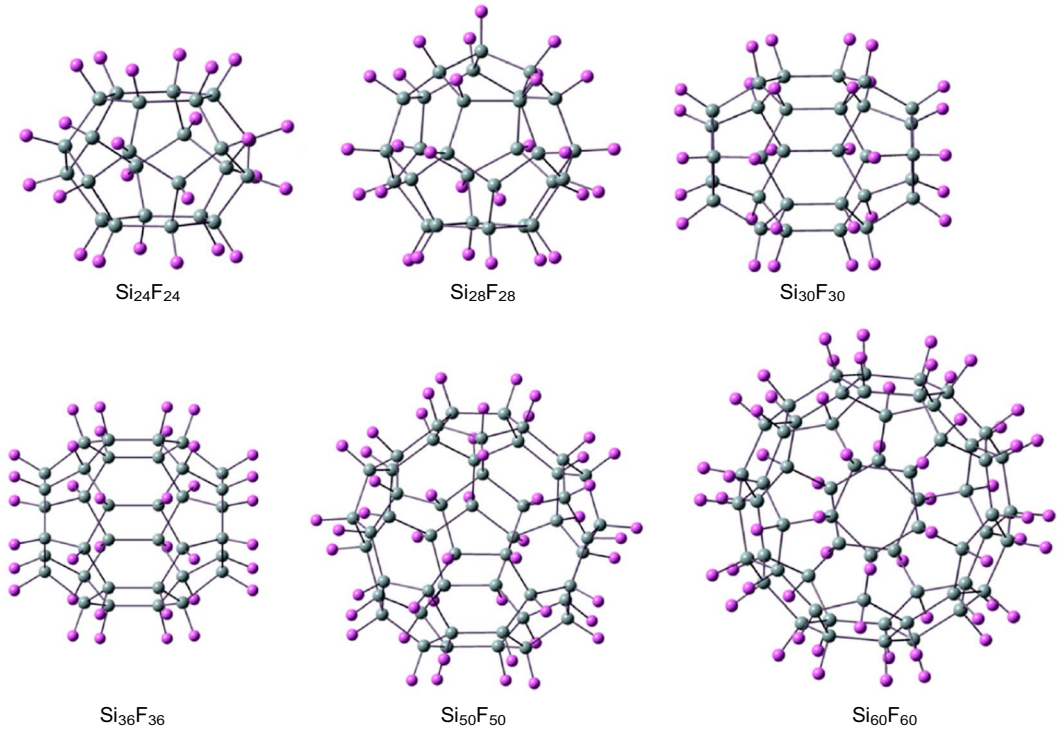


Figure 1. The spatial structures of Si_nF_n fluorinated silicon cages with $n = 24$, 28, 30, 36, 50, and 60, optimized at the B3LYP/6-311G(d,p) level. Element colours: silicon is gray, fluorine is violet. Reproduced with minor editing privilege from Anafcheh and Ghafouri[29] with the permission of *Elsevier*.

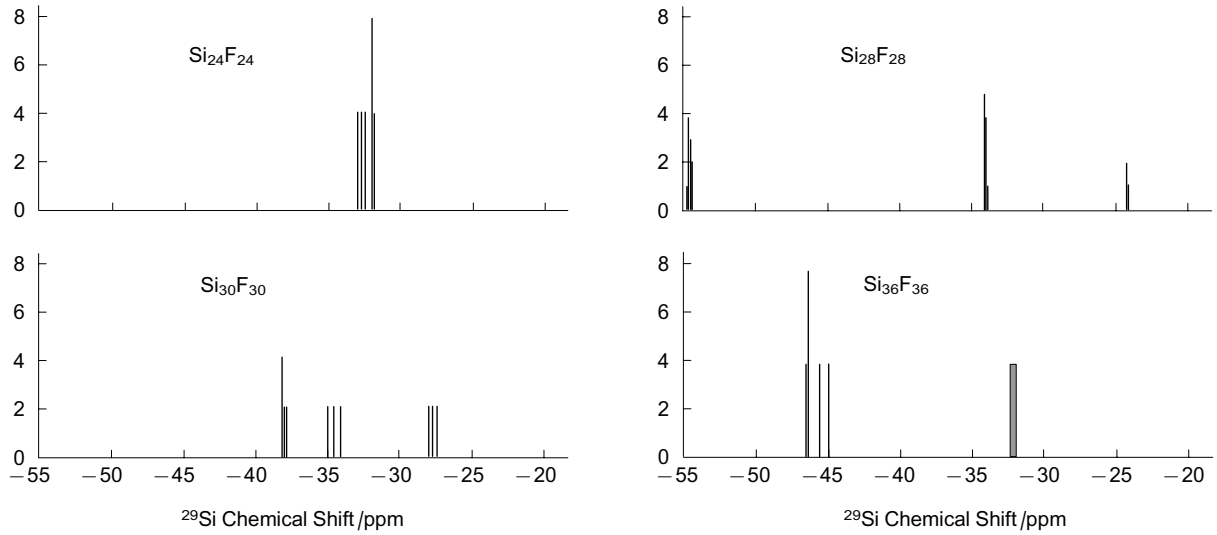


Figure 2. ^{29}Si NMR patterns with relative intensities (histograms) for Si_nF_n fluorinated silicon cages with $n = 24$, 28, 30, and 36. Reproduced with minor editing privilege from Anafcheh and Ghafouri [29] with the permission of *Elsevier*.

Molecular Orbital (LUMO) of the representative polysilanes from this series are shown in Fig. 3. It was found that there were almost no wavefunctions distributed on silicons with the HOMO orbitals, localized predominately on the Si–Si bonds of the cages, while LUMO orbitals were mostly distributed inside smaller cages and around the cage, which, by going to the larger cages, were mainly localized on the fluorine atoms. As followed from that study, calculated ^{29}Si NMR chemical shifts, as compared to experiment, provided a useful basis for the assignment of ^{29}Si resonances to different silicons in these and related cages.

Very similar, but much less representative calculations were carried out two years later by Filonenko *et al.*[30] on ^{29}Si NMR chemical shifts of silicon dioxide fullerene-like molecules in aqueous and gas phases at the DFT level with the B3LYP functional and Pople's 6-311 + G(2d,p) basis set. A reasonable agreement with experiment was reached in that study.

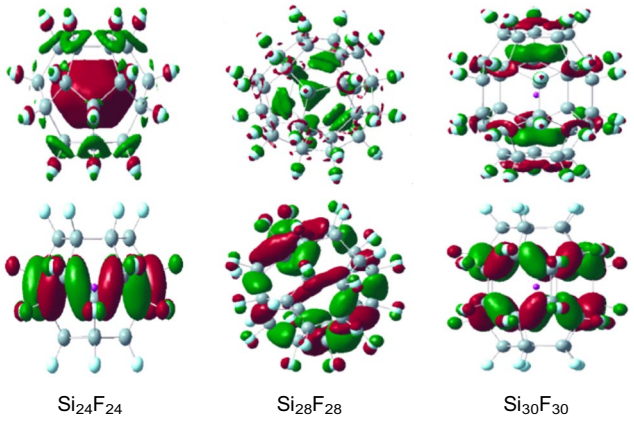


Figure 3. Molecular orbital pictures of HOMO (bottom row) and LUMO (top row) for Si_nF_n fluorinated silicon cages with $n = 24$, 28, and 30. Reproduced with minor editing privilege from Anafcheh and Ghafouri [29] with the permission of *Elsevier*.

Butler and Lewis [31] performed calculation of ^{29}Si NMR chemical shifts of as many as 37 aqueous silicate species present in zeolite at the PBE/cc-pVDZ level by incorporating solvent effects through their implicit representation using the IEF-PCM model. It was demonstrated that performed calculations could reproduce experimentally observed silicon spectra and indicated the transferability and robustness of the computation of ^{29}Si NMR chemical shifts of zeolites at this level. Complementary, a number of reassignments together with some new assignments of ^{29}Si NMR chemical shifts of some vital zeolites were proposed, based on the results of that study, to serve as a reference guide for future experimental studies in this field.

Approximately at the same period of time, Rouf and Ottosson [32] conducted a systematic DFT study of ^{29}Si NMR chemical shifts of silaphenolates and silaphenylthiolates with the most illustrative structures, solvated by potassium cation and surrounded by five molecules of tetrahydrofuran, denoted as $K^+(THF)_5$, as shown in Fig. 4. It was found that ^{29}Si NMR chemical shifts were influenced by two factors, namely by the position of the silicon atom in the ring and, on the other hand, by the substituent effect at the silicon atom. The ^{29}Si NMR chemical shifts were calculated to have the most positive values for *m*-silaphenolates, whereas those of *p*-silaphenolates were only slightly more downfield than those of the corresponding *o*-silaphenolates, displaying very weak dependence on the substituent.

It is well known that ^{29}Si NMR chemical shifts provide a remarkable sensitivity to geometrical changes, induced by intramolecular coordination and temperature effects (the latter affecting the degree of this coordination) in the series of the trigonal-bipyramidal intramolecular silicon complexes (silatranes) **1**, as established in a number of publications,[33–42] stemming from a pioneering contribution by Sidorkin, Pestunovich, and Voronkov [43] and a series of much more recent papers (see, for example, original papers [44, 45]) by a group of authors from A.N.Nesmeyanov Institute of Organoelement Compounds, Russian Academy of Sciences and N.I.Pirogov Russian National Research

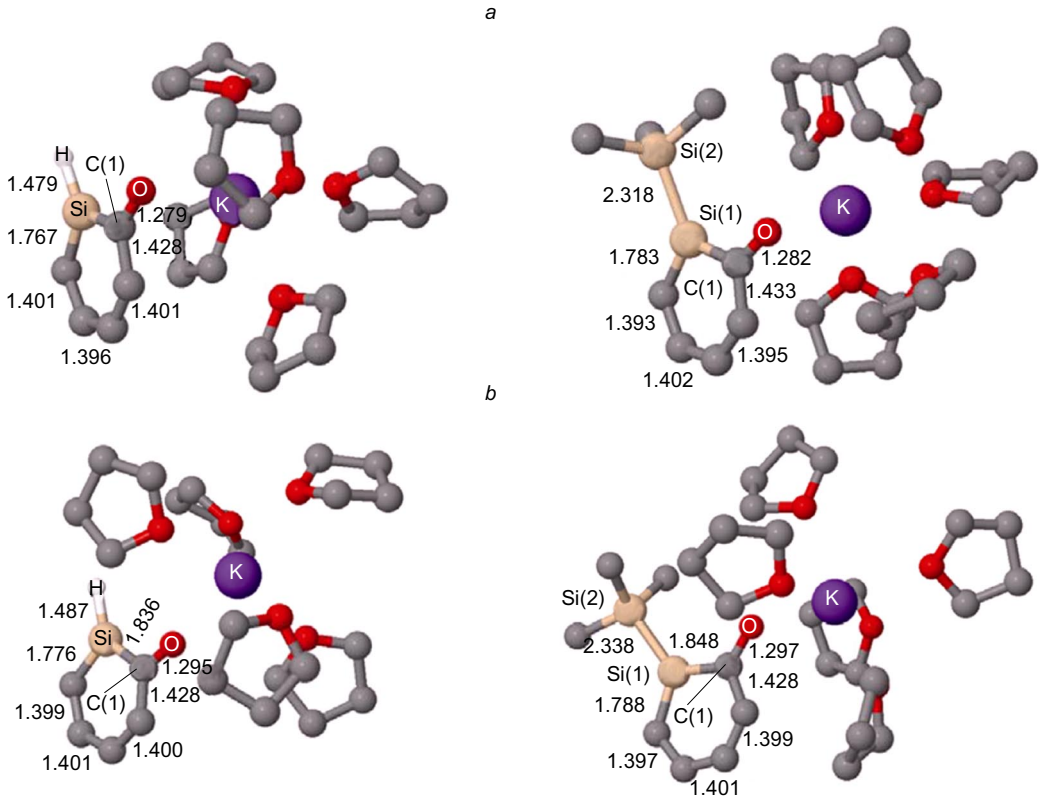
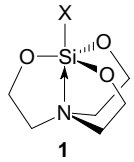


Figure 4. Geometries of mono- and disilaphenolates (accordingly, left and right structures) solvated with $K^+(THF)_5$, calculated at the DFT level using M062X (*a*) and B3LYP (*b*) functionals with Pople's 6-311G(d) basis sets. Reproduced with minor editing privilege from Rouf and Ottosson[32] with the permission, granted by an open access journal under the *Creative Commons Attribution License*.

Medical University, reviewed recently by Korlyukov and Nelyubina.[46]

As a result of these studies, it was found at the HF, MP2, and DFT levels that a significant upfield shift of a ^{29}Si NMR signal was observed with the increase of the degree of this coordination.



1

X = H, Alk, Ar, OAlk, Hal, *etc.*

In parallel with these studies, Chernyshev *et al.*[47 – 49] performed a number of calculations at the DFT level of ^{29}Si NMR chemical shifts in the series of four- five-, and six-coordinate silicon compounds. A number of functionals was tested in that study, including B3LYP, PBE0, and B1PW91, and a number of basis sets of double, triple, and quadruple zeta quality (DZP, TZP, TZ2P, and QZ4P) were examined to find out the most reliable combination of B1PW91/TZP.[47]

Calculations of ^{29}Si NMR chemical shifts in five- and six-coordinate silacyclobutane complexes, prepared from 1,1-dichlorosiletane and hydrazonic acid trimethylsilyl esters (for structures, see Fig. 5), revealed that formation of one intramolecular N → Si dative bond led to the upfield shift of the silicon resonance by about 40 ppm, while the formation of two N → Si bonds resulted in the upfield shift of as much as about 100 ppm,[48] in a good agreement with experiment. It was thus established that the coordination shift of ^{29}Si NMR resonance was an essentially additive quantity of about 50 ppm shielding per the formation of one N → Si bond in the intramolecular silicon complexes.

The latter finding was confirmed and developed further in the forthcoming publication[49] by the same principal authors dealing with the investigation of the dynamic equilibria related to the change of the coordination number of silicon in bis[*N*-(dimethylamino)imidato-*N′*,*O*]silacycloalkanes (for structures, see Fig. 6), by means of computational and experimental ^{29}Si NMR. Silacyclobutane and silacyclopentane derivatives were found to exist in solution as the mixtures of species with four-, five-, and six-coordinat silicon atoms, while silacyclohexane derivatives were found to be in the form of the mixtures of four- and five-coordinate silicon compounds, as shown in Fig. 6. Again, it was found that formation of one intramolecular N → Si bond resulted in an upfield ^{29}Si NMR shift of about 30 – 40 ppm, while the formation of two N → Si bonds induced accordingly, a shift of 90 – 110 ppm, in a very good agreement with the results of the previous study.[48]

2.1.2. Relativistic effects

It is well known that relativistic effects play an important role in the values of NMR parameters for systems with heavy atoms.[14 – 18] The importance of relativistic effects increases with increasing atomic number of a heavy atom, and besides relativistic effects in the NMR chemical shift of

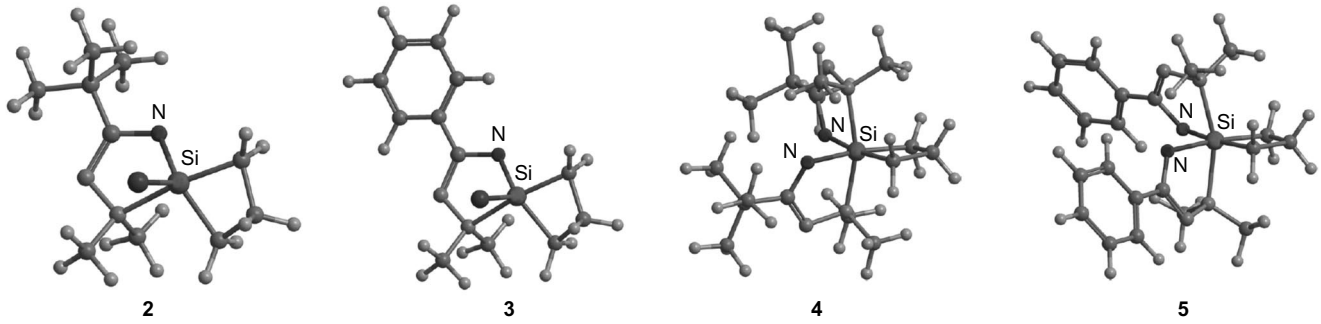


Figure 5. The structures of five- (**2**, **3**) and six-coordinate (**4**, **5**) silacyclobutane complexes, optimized at the MP2/6-311G(d,p) level. Reproduced with minor editing privilege from Chernyshev *et al.*[48] with the permission of *Springer Nature*.

a heavy atom itself, the NMR chemical shifts of light atoms adjacent to a heavy atom, are affected as well. Whereas the former effect is strongly influenced by both scalar relativistic effects and Spin–Orbit (SO) coupling, the latter tends to be dominated by the SO coupling. Both scalar spin-free relativistic effects and the SO coupling have to be imperatively considered for compounds containing heavy atoms.

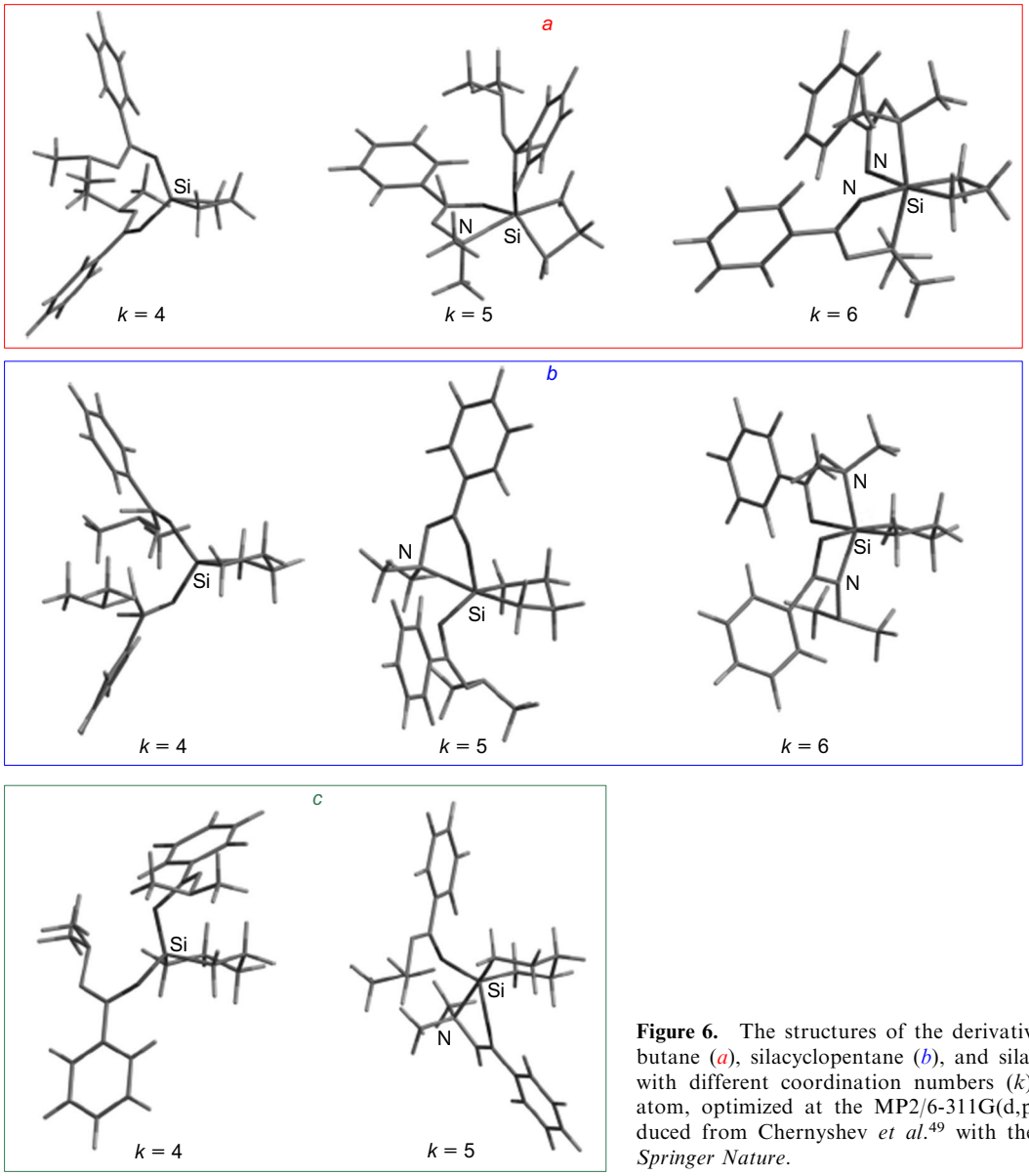


Figure 6. The structures of the derivatives of silacyclobutane (*a*), silacyclopentane (*b*), and silacyclohexane (*c*) with different coordination numbers (*k*) of the silicon atom, optimized at the MP2/6-311G(d,p) level. Reproduced from Chernyshev *et al.*[49] with the permission of *Springer Nature*.

Relativistic effects play a major role in the calculation of NMR chemical shifts and spin–spin coupling constants, provided that nuclei under consideration have heavy atoms in their nearest neighborhood. In general, relativistic effects in the values of NMR parameters include electron SO coupling (the interaction of the spin magnetic moment of an electron with the magnetic field induced by its own orbital motion) and scalar effects, the so-called Darwin term (relativistic fluctuation of an electron about its mean position), and mass–velocity corrections (relativistic increase in the mass of an electron with its velocity approaching the speed of light), which strongly affects the values of NMR shielding constants of heavy nuclei and, on the other hand, light nuclei in heavy environment. Accordingly, there are two most significant types of relativistic effects, namely the so-called scalar effects, *i.e.* the ones operators of which do not contain the electronic spin variable, and, on the other hand, the SO relativistic effects, *i.e.* those, operators of which depend on electronic spin.

Scalar effects could be defined as the sum of the mass-velocity and Darwin corrections. In its turn, mass–velocity correction arises due to the relativistic increase of the electron mass, affecting the kinetic energy of an electron, while the Darwin correction originates in the 'smearing' of the moving electron, resulting in a change of its potential energy. On the other hand, spin–orbit effect originates in the interaction of an electron spin with its own angular momentum in relation to the position of the nucleus (known as the 'one-electron effect'), or with its own angular momentum in relation to the position of another electron (known as the 'two-electron effect').

Herewith, we will not go into further details dealing with NMR relativistic effects in general, focusing primarily on the importance of relativistic effects in the values of ^{29}Si NMR chemical shifts of silicon bound to a heavy atom.

As an example, there should be mentioned a couple of early salient publications [50, 51] dealing with the manifestation of relativistic effects in ^{29}Si NMR chemical shifts of different organosilicon compounds.

Thus in the paper by Poblador-Bahamonde *et al.*[50] the ^{29}Si NMR chemical shifts in a series of closely related Ru^{II} silyl complexes have been calculated at the DFT level and compared to their experimental values. It was found that it was necessary to include the SO coupling, associated with the relativistic effects of the heavy atoms (ruthenium), for a quantitative agreement with the observed chemical shifts, but experimental trends were reasonably well reproduced, when calculations did not include this correction as well. As illustrated in Fig. 7, while accurate values were difficult to reach for the studied series of compounds shown in this figure (compare the red diamonds and black squares), a relatively good trend was found even in the absence of the SO correction (blue circles), and similar trends were obtained when different methods of including the SO correction were used. These results showed that relativistic effects, and especially the spin–orbit correction, became decisive for obtaining a fair agreement between computation and experiment. This was attributed as most likely due to the fact that the silicon atom was directly bound to ruthenium. However, the discrepancies between calculations and experiment were fairly large for all chlorosilyl groups in the considered series, indicating that not only relativistic effects were responsible for the observed trends.

Approximately at the same period of time, Zhang *et al.*[51] evaluated contributions of relativistic spin–orbit effects to

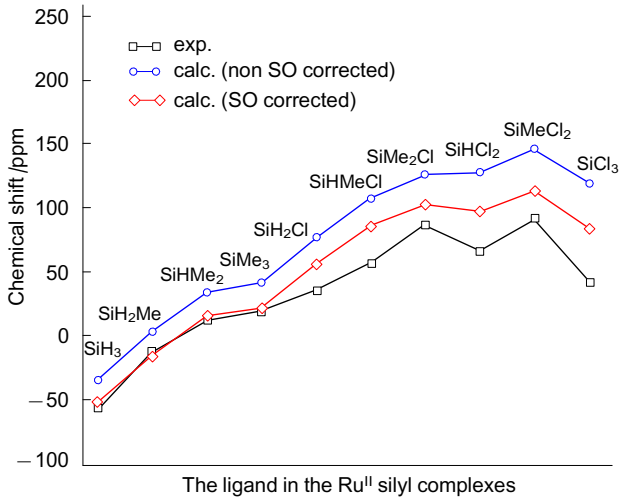


Figure 7. Experimental and computed ^{29}Si NMR chemical shifts of the representative Ru^{II} silyl complexes. Black curve (squares) are experimental values; blue curve (circles) are calculated values with scalar relativistic effects and red curve (diamonds) are calculated values including scalar and SO relativistic effects. Reproduced from Poblador-Bahamonde *et al.*[50] with minor editing privilege with the permission of the *Royal Society of Chemistry*.

the silicon magnetic shielding constants for the series of compounds $SiMe_{4-x}Cl_x$ employing a classical two-component Zeroth Order Regular Approximation (known as ZORA) formalism. It was found that SO corrections to ^{29}Si NMR chemical shifts, evaluated at the ZORA level, were required for the systems, having more than one chlorine atom directly bonded to the silicon atom. The SO corrections to ^{29}Si NMR chemical shift per chlorine substituent increased monotonously from approximately −2 ppm in $SiMe_3Cl$ to −3 ppm for $SiMe_2Cl_2$, to −4 ppm for $SiMeCl_3$, and finally to −5 ppm for $SiCl_4$. This trend was interpreted based on the analogy with the Fermi-contact mechanism of spin–spin coupling. Indeed, the increasing involvement of valence silicon *s*-type orbitals in the bonding orbitals to the chlorine substituents resulted in larger SO contributions in the series going from $SiMe_3Cl$ to $SiCl_4$. A SO correction of about −2 ppm per one chlorine substituent was thus found to be typical of different chloromonosilanes.

In three related papers by Fedorov *et al.*,[52–54] in the interim of 2015–2017, a systematic study of relativistic effects on ^{29}Si NMR chemical shifts of the diverse silanes was carried out. Using experimental ^{29}Si NMR chemical shifts as a rigorous benchmark of the performed four-component relativistic calculations, it was found[53] that taking into account relativistic effects dramatically decreased MAE of calculated ^{29}Si NMR chemical shifts *vs.* experiment. In that study, the performance of three different theoretical levels to compute ^{29}Si NMR chemical shifts of the representative series of halosilanes in comparison with experiment was applied, namely: the four-component relativistic Gauge Invariant Atomic Orbital (GIAO) DFT using KT3 functional (GIAO-DFT-KT3) and GIAO within the Random Phase Approximation (GIAO-RPA). Also, a hybrid scheme of the nonrelativistic GIAO-MP2 taking into account relativistic corrections at the four-component relativistic GIAO-RPA level was employed. This is illustrated in Fig. 8, taken from the title publication.

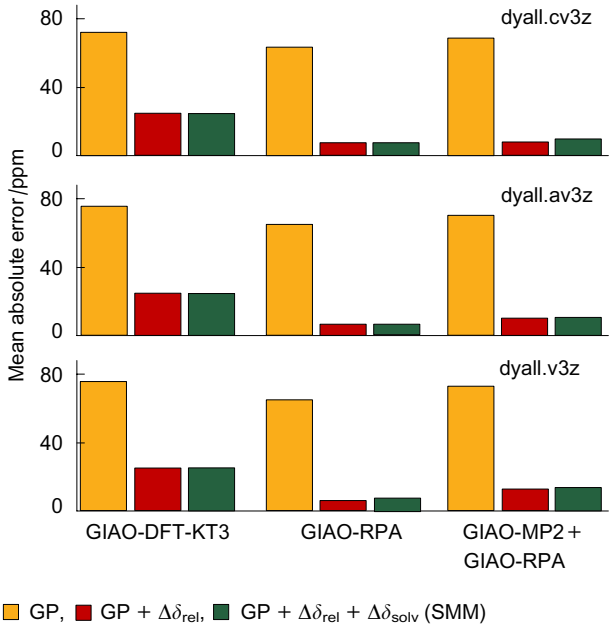


Figure 8. Mean absolute errors of ^{29}Si NMR chemical shifts of the representative series of silanes, calculated with using the GIAO-DFT-KT3, GIAO-RPA, and GIAO-MP2 methods: in gas phase at the nonrelativistic level (yellow bars); in gas phase taking into account relativistic effects (red bars); and in liquid phase taking into account relativistic effects (green bars). Different Dyall's basis sets of triple zeta quality were used throughout. Implied abbreviations and/or notations are as follows: GP is gas phase; $\Delta\delta_{rel}$ is relativistic correction to chemical shift; $\Delta\delta_{solv}$(SSM) is solvent correction to chemical shift evaluated within the supermolecular solvation model. Reproduced from Fedorov *et al.*[53] with the permission of the *American Chemical Society*.

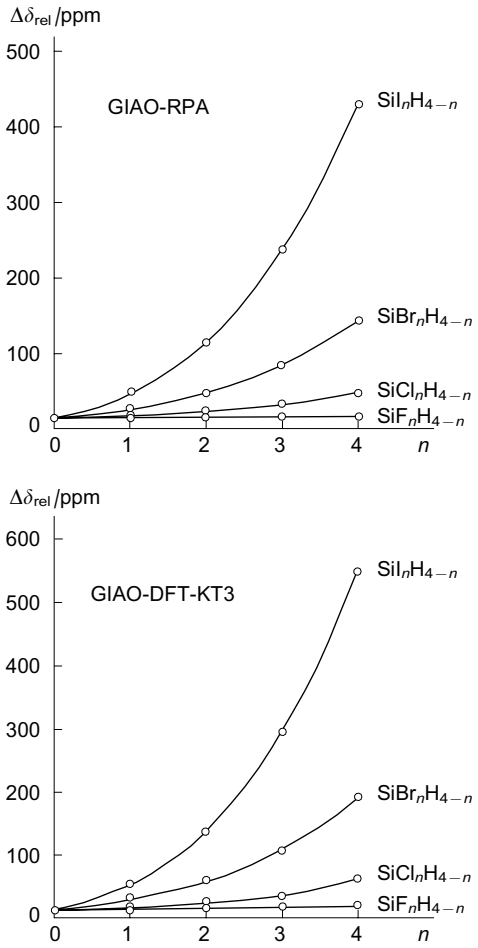


Figure 9. Relativistic contribution to ^{29}Si NMR shielding constant as a function of a number of halogen atoms attached to silicon, calculated at the RPA and DFT levels within a full four-component relativistic Dirac's scheme with using the dyall.av3z basis set. Reproduced from Fedorov *et al.*[53] with the permission of the *American Chemical Society*.

In each case, the authors applied three different relativistic Dyall's basis sets, namely valence, dyall.v3z, diffuse valence, dyall.av3z, and core valence, dyall.cv3z, taking into account solvent effects (chloroform) within the supermolecular solvation model at the nonrelativistic GIAO-DFT-KT3 level. It was found that MAE decreased from about 75 ppm to about 20–25 ppm for the four-component relativistic GIAO-DFT-KT3 method and to about 10–15 ppm for the four-component relativistic GIAO-RPA method together with a combined scheme of nonrelativistic GIAO-MP2 with the four-component relativistic GIAO-RPA. Either diffuse or core functions in Dyall's diffuse valence basis sets surprisingly showed no effect, as compared to the valence ones. Also it was found that taking into account solvent effects (chloroform) in those calculations did not affect noticeably the accuracy of any of the tested methods.

It is seen in Fig. 9, taken from the same publication,[53] that relativistic contribution rapidly increased with the number of halogens, and noteworthy, this increase was not linear. It was found that this tendency was most pronounced in the iodosilanes series: at the GIAO-DFT-KT3/dyall.av3z level, relativistic contribution of the first iodine atom was about 52 ppm, that of the second iodine was 85 ppm, that of the third iodine was 156 ppm, and that of the fourth one amounted to as much as 258 ppm!

A general conclusion, following from that study of relativistic effects in ^{29}Si NMR absolute shielding constants of halosilanes, was that they were next to negligible (up to several ppm) in fluorosilanes, noticeably larger (up to several dozens of ppm) in chlorosilanes, much larger (up to 200 ppm) in bromosilanes, and remarkably large (several hundreds of ppm!) in iodosilanes. Thus, it followed that nonrelativistic calculations of ^{29}Si NMR absolute shielding constants (chemical shifts) were adequate for fluorosilanes, admissible for chlorosilanes, and absolutely inadequate and unacceptable for halosilanes bearing at least one atom of either bromine or iodine attached to a silicon atom. For the latter, only relativistic level was appropriate, better that within a full four-component relativistic Dirac's theory, as compared to the two-component quasi relativistic scheme.

2.2. Solid state

A rather specific area of silicon NMR is that of computational ^{29}Si NMR in solids, which could be exemplified by some illustrative original publications[55–58] together with the reviews by Charpentier *et al.*[59] and Pedone.[60]

As an example of these studies, there might be cited a milestone paper[57] devoted to probing silicon and aluminium chemical environments in silicate and aluminosilicate glasses by solid state ^{29}Si Magic Angle Spinning (MAS) NMR spectroscopy together with the accurate first-principles calculations. Studied in that paper

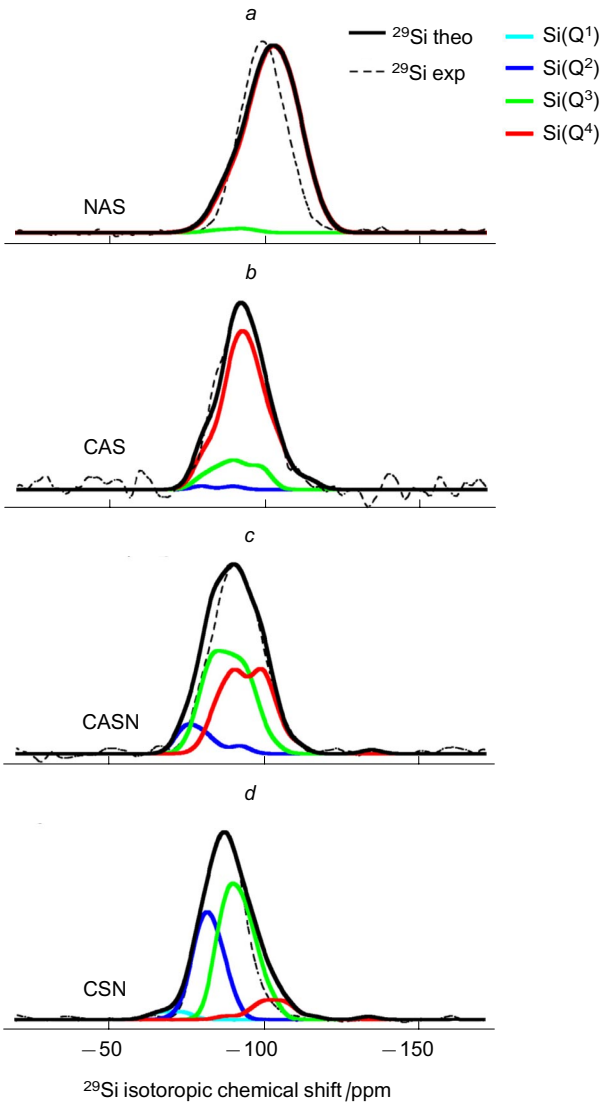


Figure 10. Comparison between experimental and theoretical (black solid lines) ^{29}Si MAS NMR spectra, normalized to the same maximum height for (*a*) NAS, (*b*) CAS, (*c*) CASN and (*d*) CSN glasses. The individual contributions of the Q^n species to the total theoretical spectra are reported in coloured solid lines, see original publication for details. Reproduced from Gambuzzi *et al.*[57] with the permission of *Elsevier*.

were silicate glass, $60\,SiO_2 \cdot 20\,Na_2O \cdot 20\,CaO$ (CSN), and three aluminosilicate glasses, $60\,SiO_2 \cdot 20\,Al_2O_3 \cdot 20\,CaO$ (CAS), $78\,SiO_2 \cdot 11Al_2O_3 \cdot 11Na_2O$ (NAS), and $60SiO_2 \cdot 10\,Al_2O_3 \cdot 10\,Na_2O \cdot 20\,CaO$ (CASN). Theoretical and experimental ^{29}Si MAS NMR spectra, obtained in that study, are shown in Fig. 10. It was found that, whereas experimental peaks showed roughly a Gaussian distribution shape, theoretical ones exhibited more accentuated asymmetries, which was explained by the authors in terms of the limited number of silicon atoms used in the simulation. All calculations of ^{29}Si MAS NMR spectra of NAS, CAS, CASN, and CSN glasses were performed at the DFT level using the Perdew – Burke – Ernzerhof (PBE) exchange-correlation functional for light atoms and an ultrasoft pseudopotential ($3s^23p^2$) for silicon.

Figure 11 shows correlation plots of isotropic ^{29}Si NMR chemical shifts and the Si – O – X (X = Si or Al) intertetrahedral angles in all four studied types of glasses, NAS, CAS, CASN, and CSN. Based on these data, it was found [57] that correlation coefficients in CASN glass were lower than those in CSN glass, suggesting that aluminium, as well as calcium, may contribute to the weakening of correlations between the isotropic ^{29}Si NMR chemical shifts and the Si – O – X intertetrahedral angles.

Another very recent example of related studies, performed by Charpentier *et al.*,[55] deals with the investigation of structure of strontium aluminosilicate glasses by means of molecular dynamics simulation, neutron diffraction, and solid-state ^{29}Si NMR. Figure 12 shows the ^{29}Si MAS NMR spectra, the variations of the mean isotropic chemical shift, and the widths of the spectra. Dashed lines represent the linear regression of the isotropic chemical shifts on specific ranges of composition. It was found, that for both glass series, the increase of silica content yielded a decrease of the isotropic chemical shift and an increase of the spectrum width.

Along with considerable variation of the isotropic ^{29}Si NMR chemical shift, both glass series showed a significant increase of the widths of their spectra against the silica content. Based on these results, it was suggested [55] that the short- and medium-range structures had a different NMR response to the local disorder, so that it might be characterized by a different line width even for a similar bond angle distribution around each environment, rather than an increased local disorder around SiO_4 units for lower aluminium and strontium content.

One more example deals with an earlier contribution from Evans *et al.*,[58] related to the ^{29}Si MAS NMR investigation of three samples from the dumortierite group of minerals, namely a dumortierite, consisting of the dark blue euhedral crystals from Madagascar (D34); a fine-grained pale blue dumortierite from British Columbia (D12); and a creamy white holtite from Poland (WPH). The RHF calculations of the ^{29}Si MAS NMR chemical shifts of D34, D12, and WPH were performed on model clusters, exemplified in Fig. 13 for the $SiAl_8O_{35}H_{42}$ structure, consisting of the third shell of atoms around the central silicon atom. The goal of the performed calculations was primarily the matching of the local environments of silicon atoms to peaks in the solid-state ^{29}Si MAS NMR spectra. Basically, it was shown that both silicon sites in the dumortierite structure were distinguishable in the ^{29}Si MAS NMR spectrum of D34 and D12, although they were not in the closely related holtite structure (WPH), where the disorder effects markedly broadened individual signals.

3. Computation of spin – spin coupling constants involving the ^{29}Si nucleus

The second half of the present review deals with the computation of spin – spin coupling constants, involving silicon, in most part, ^{29}Si – ^{1}H and ^{29}Si – ^{13}C. These calculations are much less common than those of ^{29}Si NMR chemical shifts, so that, herewith, we will concentrate only on several most illustrative examples.

3.1. Spin – spin coupling constants ^{29}Si – ^{1}H

In the early paper by Malkina *et al.*[61] (which may be called a rather 'historical' one), the one-bond ^{29}Si – ^{1}H coupling constants of different silanes were calculated at the DFT level, as described in their earlier publications,[62] using Vosko, Wilk, and Nusair's exchange-correlation functional (VWN); Becke's exchange with Perdew's correlation functional (BP); and Perdew and Wang's exchange-correlation

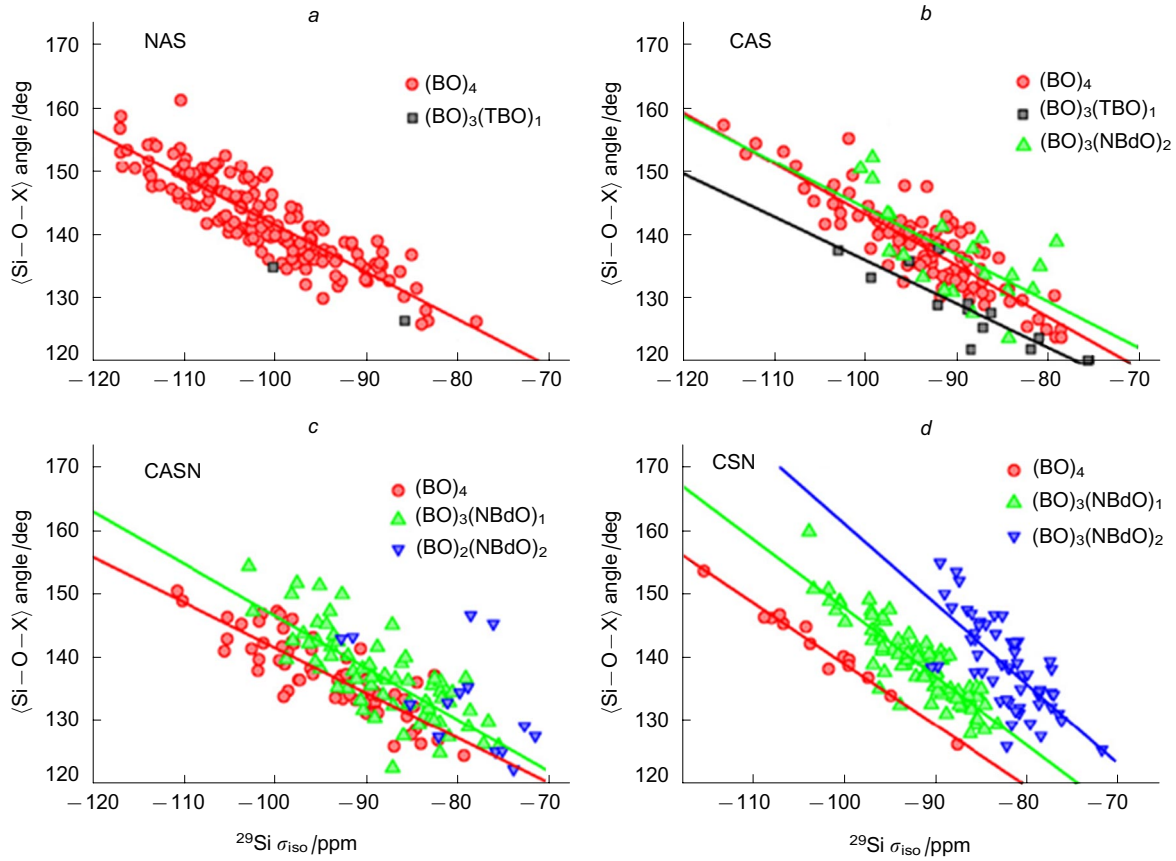


Figure 11. Plot of isotropic ^{29}Si NMR chemical shifts *vs.* the Si–O–X intertetrahedral angles for different connectivity environments of silicon in (*a*) NAS, (*b*) CAS, (*c*) CASN and (*d*) CSN glasses. Linear regression fitting lines are also shown with coherent colours as visual guides. BO is bridging oxygen atom, NBdO is non-bridging oxygen atom, TBO is triple bridging oxygen atom. Reproduced from Gambuzzi *et al.*[57] with the permission of *Elsevier*.

functional (PW91). The Kutzelnigg's IGLO-III basis set and very large, fully uncontracted, basis sets of Partridge (UP) were employed, as exemplified in Table 1 for the series of the most representative compounds **6**–**12** from this series. It is seen that couplings calculated with the IGLO-III basis set are shifted by about 7%–11% from their experimental values, while those evaluated with the UP basis set are in an excellent agreement with experiment. Also, it was found that relativistic effects in the title set of compounds **6**–**12** (not taken into account at that level) were also important for spin–spin couplings, including even such relatively 'light' element as silicon.

In addition to these data, ten years later Deng, Cheeseman and Frisch[63] computed the value of $^1J_{Si,H}$ in the unsubstituted silane, SiH_4, to be −209.9 Hz, as compared to the experimental value of 202.5 Hz in gas phase.[64] In this study, they used the uncontracted UGBS2P basis set, including two additional polarization functions for each function in the parent UGBS basis set:[65] one *p* and one *d* function for each *s* function and one *d* and one *f* function for each *p* function.

At approximately the same period of time, correlated *ab initio* calculations were reported by Sauer and Raynes[66, 67] of $^1J_{Si,H}$ coupling constant in silane, SiH_4, which showed that stretching one of the Si–H bonds from its equilibrium value increased the one-bond silicon–hydrogen coupling constants of the other three bonds by more than the increase of that of the stretched bond. This phenomenon was referred to by the authors as 'the unexpected differential sensitivity of the silicon–hydrogen bonds'.

Table 1. Total values of $^1J_{Si,H}$ spin–spin coupling constants in a number of representative compounds, calculated at the DFT level in comparison with experimental data. All values are in Hz. Compiled from Malkina *et al.*[61]

Compound	Formula	IGLO-III	UP	Exp.
6	SiH_3Me	−179.5	−196.9	−194.3
7	SiH_2Me_2	−174.3	−189.8	−188.6
8	SiH_3SiH_3	−181.1	−198.3	−198.2
9	SiH_3F	−212.1	−232.7	−229.0
10	SiH_2F_2	−258.8	−282.3	−282.0
11	$SiHF_3$	−347.3	−379.5	−381.7
12	SiH_3CN	−212.7	−232.0	−238.7

Much later, Ambati[68] performed DFT B3LYP/6-31G calculations of $^2J_{Si,H}$ and $^2J_{H,H}$ coupling constants in the fully hydrolyzed form of bis(trihydroxysilaylethane) **13**. It was found that title couplings remained fairly constant with free rotation, as expected. However, $^3J_{Si,H}$ and $^3J_{H,H}$ in the bridge depended on the Si–C–C–Si dihedral angle of the bridging group backbone. Figure 14 shows variation of these coupling constants with the dihedral angle in the bridging group of compound **13**.

$(HO)_3Si-CH_2-CH_2-Si(OH)_3$
13

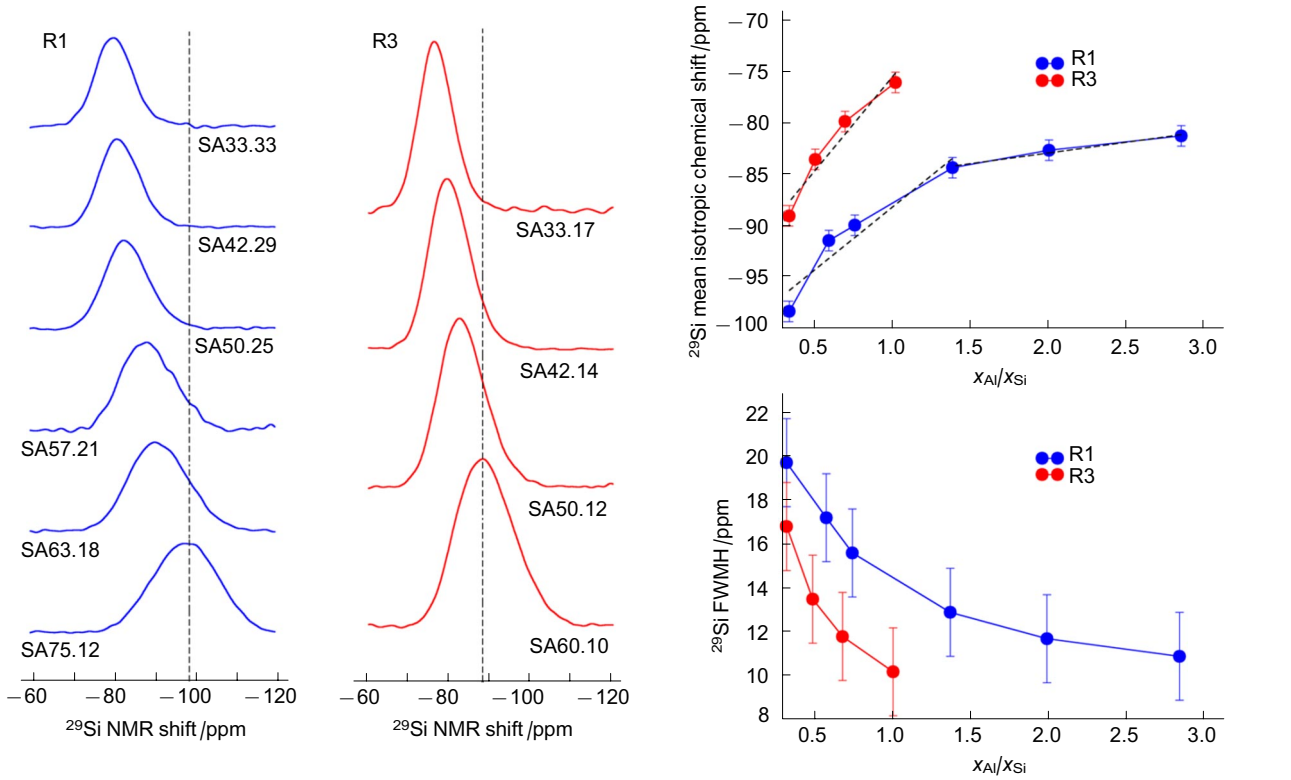


Figure 12. Left panel: experimental ^{29}Si MAS NMR spectra of the strontium aluminosilicate glasses. Right panel: Variation of the isotropic chemical shift (centre of gravity, top) and the spectral width (full width at middle-height, bottom) against the glass composition. The following notations and abbreviations are used: FWMH is full width at middle-height; R1 are strontium glasses with the composition $(SiO_2)_{1-2x}(Al_2O_3)_x(SrO)_x$; R3 is strontium glasses with the composition $(SiO_2)_{1-4x}(Al_2O_3)_x(SrO)_{3x}$; SA33.33, SA42.29, SA50.25, SA57.21, SA63.18, SA75.12, SA33.17, SA42.14, SA50.12 and SA60.10 are strontium glasses with different composition of aluminium, oxygen, silicon, and strontium, see original publication for details. Reproduced from Charpentier *et al.*[55] with the permission of the *American Chemical Society*.

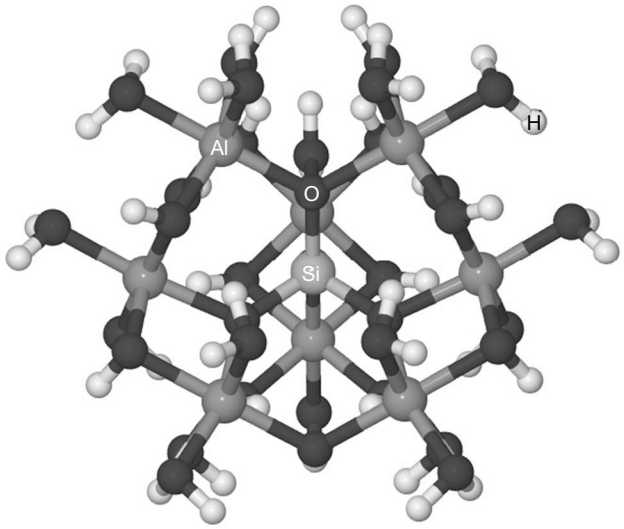


Figure 13. The model cluster $SiAl_8O_{35}H_{42}$, consisting of the third shell of atoms around the central silicon atom. Reproduced with minor editing privilege from Evans *et al.*[58] with the permission of the *Mineralogical Society of America*.

Fitting these curves to a general Karplus equation, $J(\varphi) = A\cos^2\varphi + B\cos\varphi + C$ (where φ is the corresponding dihedral angle), resulted in the following equations, describing dihedral angle dependencies of $^3J_{Si,H}$ and $^3J_{H,H}$:

$$^3J_{Si,H} = -14.9\cos^2\varphi + 3.1\cos\varphi - 0.4 \quad (1)$$

$$^3J_{H,H} = 14.9\cos^2\varphi + 0.8\cos\varphi + 0.5 \quad (2)$$

Further simulation of ^{29}Si NMR spectra, based on $^3J_{Si,H}$ and $^3J_{H,H}$ couplings, performed by Ambati and Rankin,[69] enabled unambiguous spectral assignment of **13** and related species, based on the iterative matching of calculated and experimental spectra, as illustrated in Fig. 15 for compound **13**. It followed that theoretical calculation of silicon-hydrogen couplings, performed at a simple DFT level, provided an efficient tool in structural elucidation of hydroxysilylethanes and related organosilicon compounds.[69]

Several years later Rusakov *et al.*[70–72] performed a series of the Second-Order Polarization Propagator Approach (SOPPA) calculations, SOPPA(MP2), SOPPA(CC2), and SOPPA(CCSD), of the one-bond, geminal, and vicinal silicon – hydrogen couplings in the series of alkenylsilanes,[70] alkenylmethylsilanes,[71] and halosilanes,[72] which was reviewed later.[73]

In the first paper from this series,[70] the benchmark calculations of geminal and vicinal ^{29}Si – ^{1}H spin – spin coupling constants across the double bond in the series of alkenylsilanes have been performed at both DFT and SOPPA levels in comparison with experiment. At the former, four density functionals, B3LYP, B3PW91, PBE0, and KT3, were tested in combination with five representative basis sets, namely those of Dunning, cc-pVXZ (X = D, T), together with those augmented with tight

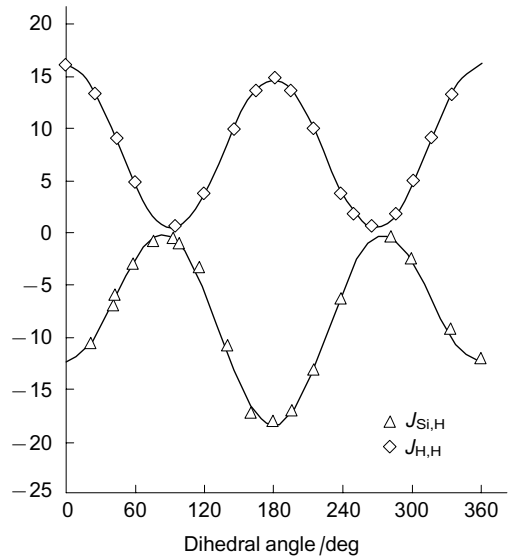


Figure 14. Variation of $^3J_{Si,H}$ and $^3J_{H,H}$ in the bridging group of bis(trihydroxysilaylethane) **13** with the Si–C–C–H and H–C–C–H dihedral angles. Points represent the values obtained from the DFT calculations, while curves represent their Karplus fits. Reproduced with minor editing privilege from the Ph.D. Dissertation of Ambati[68] with the permission of the author.

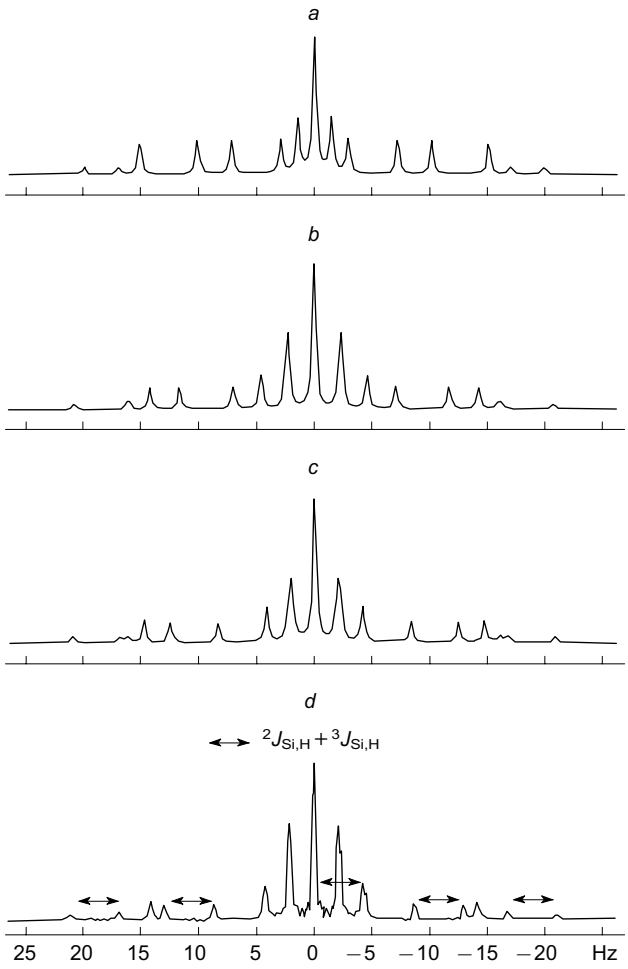


Figure 15. Simulated ^{29}Si NMR spectra of bis(trihydroxysilaylethane) **13** (*a*–*c*), compared to its experimental spectrum (*d*). Coupling constants for the theoretically derived spectra (*a*, *b*) are obtained at either B3LYP or AM1 levels with the regression (*c*) to better fit with experiment. Splittings marked in experimental spectrum are those due to the geminal and vicinal couplings between silicon and hydrogen. Reproduced from Ambati and Rankin[69] with the permission of the *American Chemical Society*.

s-functions, cc-pVXZ-su2 (X = D, T), and also that of Sauer, aug-cc-pVTZ-J. The same basis sets were also used in all SOPPA calculations — SOPPA(MP2) or simply SOPPA, SOPPA(CC2), and SOPPA(CCSD). These results are presented graphically in Fig. 16. On the whole, the wavefunction-based SOPPA methods showed better performance, as compared to the DFT calculations, with the most efficient combination of SOPPA(MP2)/cc-pVTZ-su2, characterized by a mean absolute error of only 0.4 Hz with a span of about 40 Hz. On the whole, the overall contribution of the non-contact terms was shown to be almost negligible in most cases. Out of the three non-contact interactions, only the spin–orbit mechanism was of any practical meaning, giving a minor contribution of up to 0.3 Hz (in absolute value) to the total values of calculated $J_{Si,H}$, while the spin–dipolar term was beyond 0.1 Hz in all cases.

Out of the four DFT functionals examined in that paper[70] and presented in Fig. 16, the PBE0 demonstrated the best performance with the Mean Absolute Error (MAE) of about 1 Hz, while KT3 and B3PW91 showed much worse results with the MAE of about 3–4 Hz. At the same time, the B3LYP functional was characterized by a MAE of approximately 1.5 Hz. For the wavefunction-based SOPPA methods, the SOPPA(MP2) and SOPPA(CC2) demonstrated very good performance with the MAE of less than 0.5 Hz, which was, indeed, a very encouraging result of that study. Surprisingly, SOPPA(CCSD) didn't show any improvement and even performed slightly worse, as compared to the parent SOPPA(MP2) method.

In the second paper,[71] the authors performed calculations of geminal and vicinal ^{29}Si–^{1}H spin–spin coupling constants across and 'roundabout' double bond in the series of alkenylmethylsilanes and alkenylchlorosilanes at the SOPPA(MP2) level in a good agreement with experiment. To analyze structural trends of $^2J_{Si,H}$ in this series, they applied the Natural J-Coupling (NJC) analysis, developed by Wilkens and coworkers[74] and independently by Peralta, Contreras and Snyder[75] for the interpretation of scalar spin–spin coupling constants in terms of the Natural Bond Orbitals (NBO) approach of Weinhold.[76]

Two structural trends, namely the geometry of the coupling pathway and the effect of the electron-withdrawing substituent, have been explained in terms of the NJC analysis within the framework of the NBO approach. Thus, the marked difference between cisoidal and transoidal ^{29}Si–^{1}H spin–spin coupling constants across double bonds accounted for the hyperconjugative contributions, including bonding and antibonding Si–C and C–H orbitals, while the main portion of the chlorine effect was interpreted in terms of the Lewis (steric) contributions, including bonding Si–Cl orbitals, as shown in Fig. 17.

It was thus shown[71] that Lewis (steric) terms dominated over the delocalization terms in the overall sum of the principal NJC contributions of all three ^{29}Si–^{1}H coupling constants, $^2J_{gem}$, $^3J_{cis}$ and $^3J_{trans}$. However, delocalization terms were of particular significance to account for a marked difference between cisoidal and transoidal ^{29}Si–^{1}H vicinal couplings, $^3J_{cis}$ and $^3J_{trans}$, while for

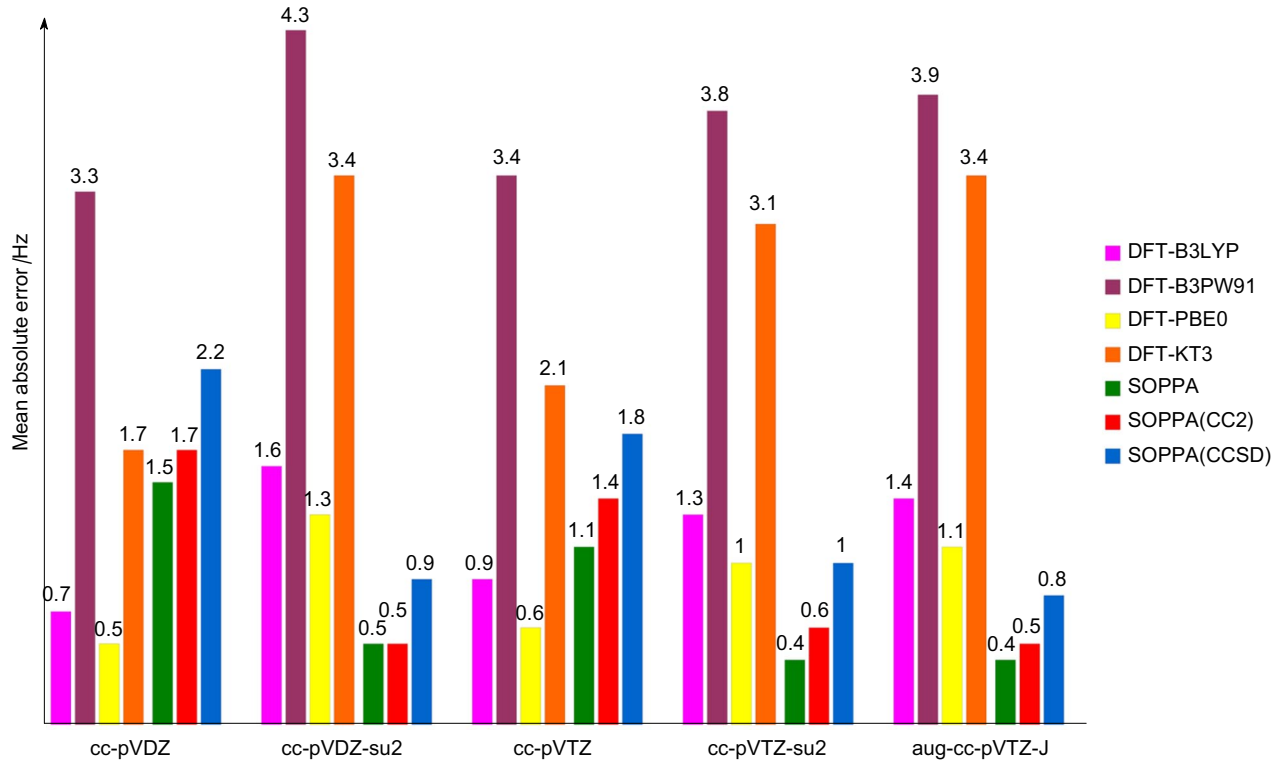


Figure 16. Mean absolute errors of different DFT and SOPPA methods, used in combination with different basis sets, derived from the benchmark calculations of $^{29}Si-^{1}H$ spin–spin coupling constants in the series of alkenylsilanes. Reproduced from Rusakov *et al.*[70] with the permission of *John Wiley and Sons*.

geminal $^{29}Si-^{1}H$ coupling constants, $^{2}J_{gem}$, delocalization terms together with all three remaining terms, Lewis, delocalization, and repolarization contributions, essentially compensated each other.

In the third paper in this series,[72] the one-bond $^{29}Si-^{1}H$ spin–spin coupling constants were calculated at the DFT, SOPPA(MP2), SOPPA(CC2), and SOPPA(CCSD) levels in the series of halosilanes, SiH_nX_{4-n} (X = F, Cl, Br and I), with a special focus on relativistic effects and vibrational corrections. At the non-relativistic level, the wavefunction methods showed much better results, as compared to those of DFT, with a Mean Absolute Percentage Error (MAPE) of about 2%. At the DFT level, out of the four tested functionals, B3LYP, PBE0, KT2, and KT3, the Perdew, Burke, and Ernzerhof's PBE0 showed best performance characterized by the MAPE of about 2.5%. However, other functionals, especially those of Keal and Tozer, KT2 and KT3, were characterized with much higher MAPE, reaching as much as 15%. Taking into account relativistic effects and vibrational corrections noticeably improved the wave-function method results, especially those of SOPPA(CCSD), but slightly worsened the DFT-PBE0 performance. All mentioned tendencies in the performed calculation of the one-bond $^{29}Si-^{1}H$ spin–spin coupling constants of halosilanes are demonstrated in Fig. 18, taken from the original publication.[72] For the most efficient SOPPA(CC2) method, the achieved mean average error was as small as 2.8 Hz for a changing of $^{1}J_{Si,H}$ of around 200 Hz, and this was indeed a very encouraging result for the future studies in this field.

In two very recent and closely related publications by Scherer and coworkers,[77,78] together with some earlier contributions from the same group,[79,80] a detailed structural investigation of the non-classical transition-metal silane complexes, exemplified with the structures **14**–**24** shown in Fig. 19, has been performed by a combined experimental and theoretical study of their through-bond

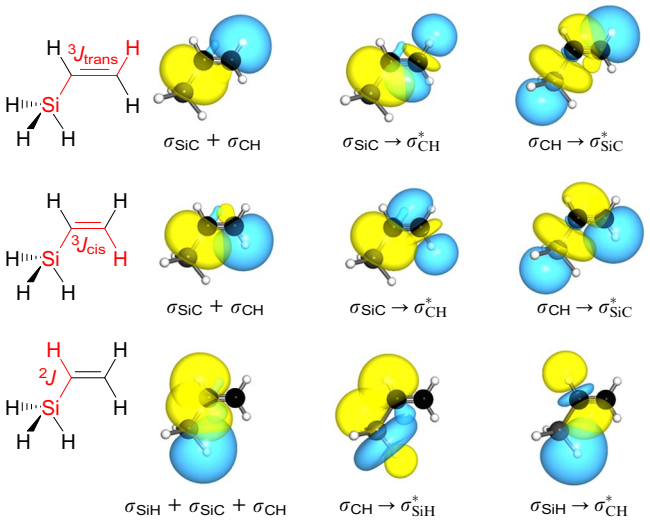


Figure 17. Principal NJC contributions to geminal and vicinal $^{29}Si-^{1}H$ spin–spin coupling constants across and roundabout double bond of vinylsilane. For the notations, see original paper. Reproduced from Rusakov *et al.*[71] with the permission of *John Wiley and Sons*.

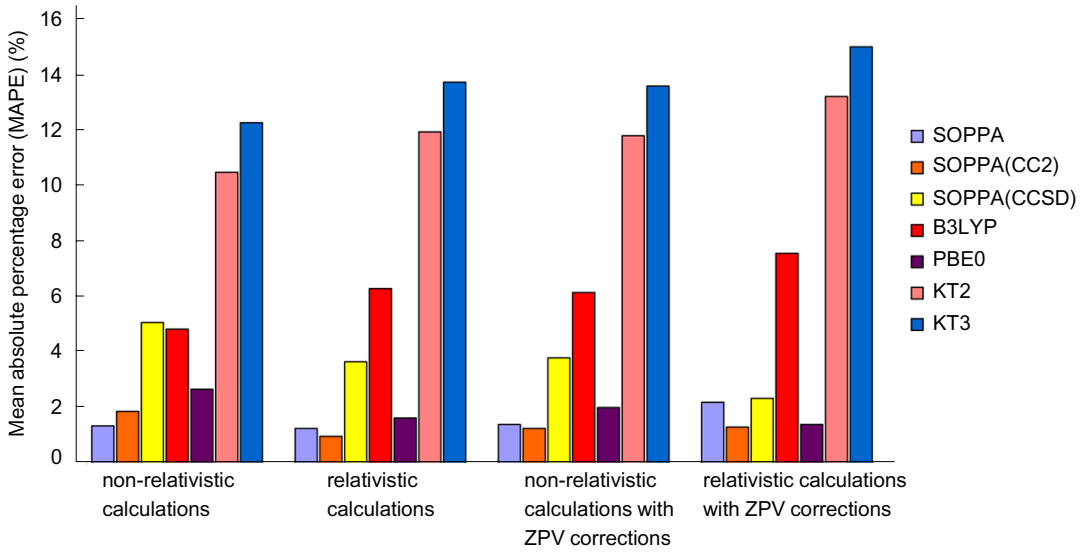


Figure 18. Mean absolute percentage errors of different DFT and SOPPA methods *vs.* experiment, derived from the benchmark calculations of the one-bond $^{29}Si-^{1}H$ spin–spin coupling constants in the series of halosilanes. Reproduced from Rusakov *et al.*[72] with the permission of *John Wiley and Sons*.

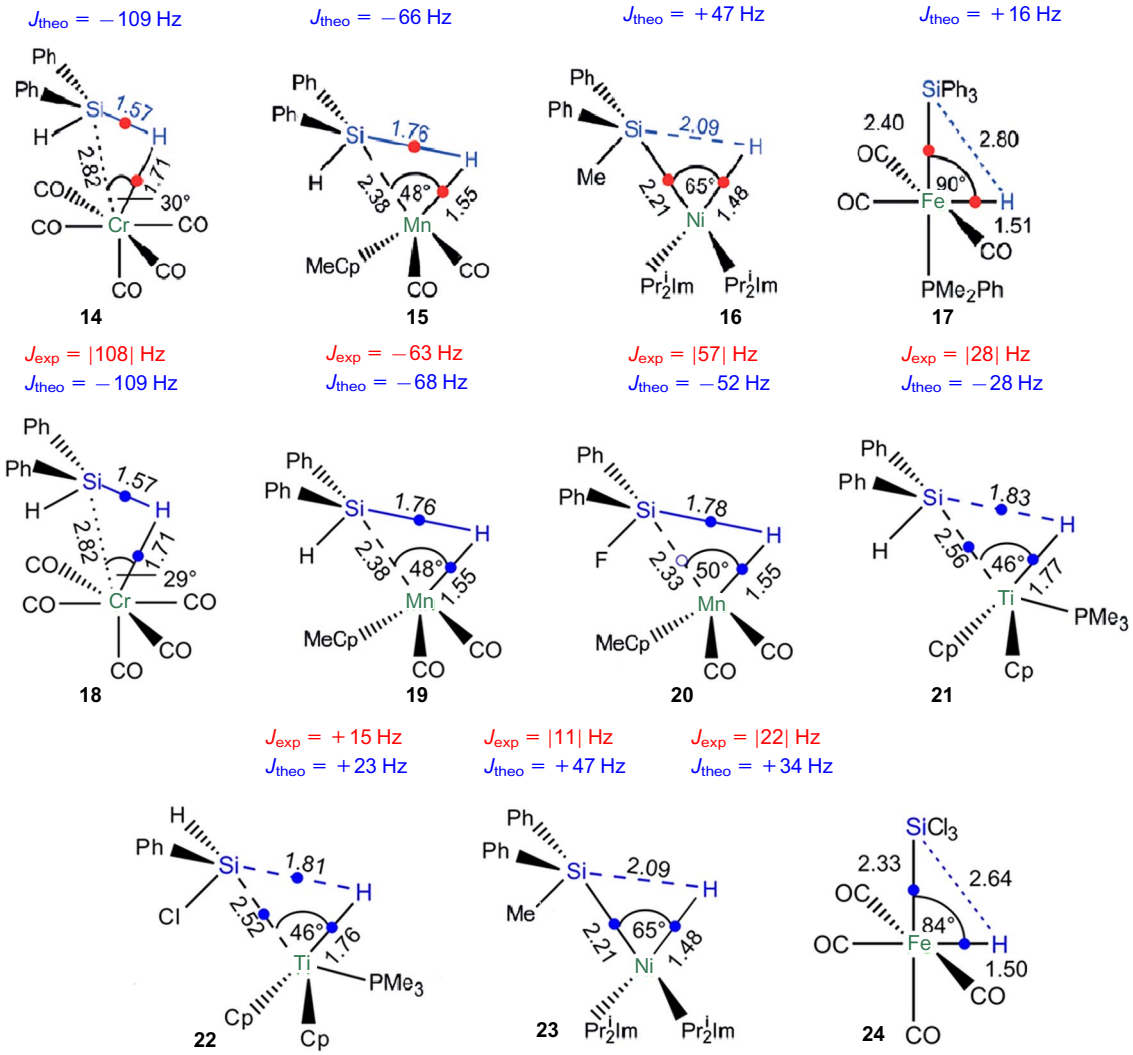


Figure 19. Interatomic and bond distances, bond critical points, and experimental and calculated $J_{Si,H}$ spin–spin coupling constants of silane complexes with the transition metals — chromium, manganese, nickel, titanium, and iron. Reproduced with minor editing privilege from Scherer *et al.*[77] with the permission of *John Wiley and Sons* and from Meixner *et al.*[78] with the permission of the *American Chemical Society*.

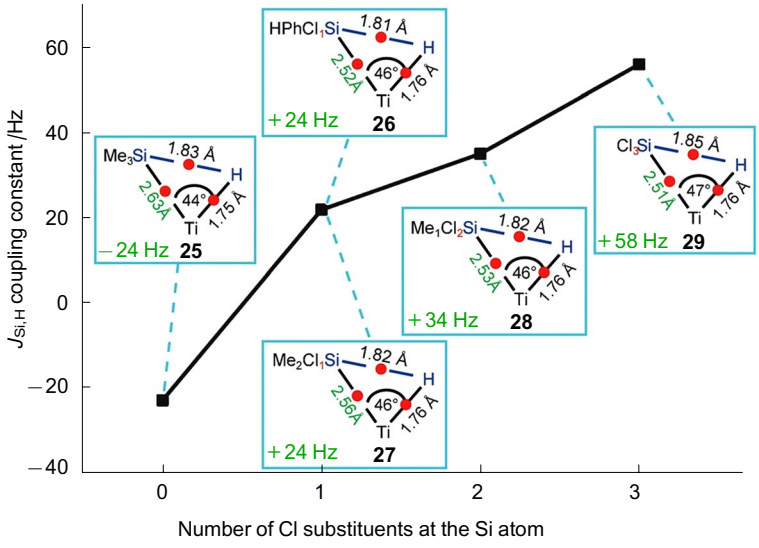


Figure 20. Interatomic and bond distances, bond critical points, and calculated $J_{Si,H}$ spin – spin coupling constants of the silane complexes with titanium as a function of the number of chlorine substituents at the silicon atom. Reproduced from Scherer *et al.*[77] with minor editing privilege with the permission of *John Wiley and Sons*.

and through-space contributions (and combination of both ones) to silicon – hydrogen spin – spin coupling constants.

One of the intriguing aspects of the silicon – hydrogen coupling constants in these series is their absolute signs. It is seen in Fig. 20 that calculated values of $J_{Si,H}$ in the series of **25** – **29** change their sign from negative in **25** to positive in **26** – **29**, as the number of chlorine substituents increases, which simultaneously reduces the Ti – Si bond length and enhances the completion of the oxidative addition process. The Si – H bond lengths and corresponding Si – Ti – H

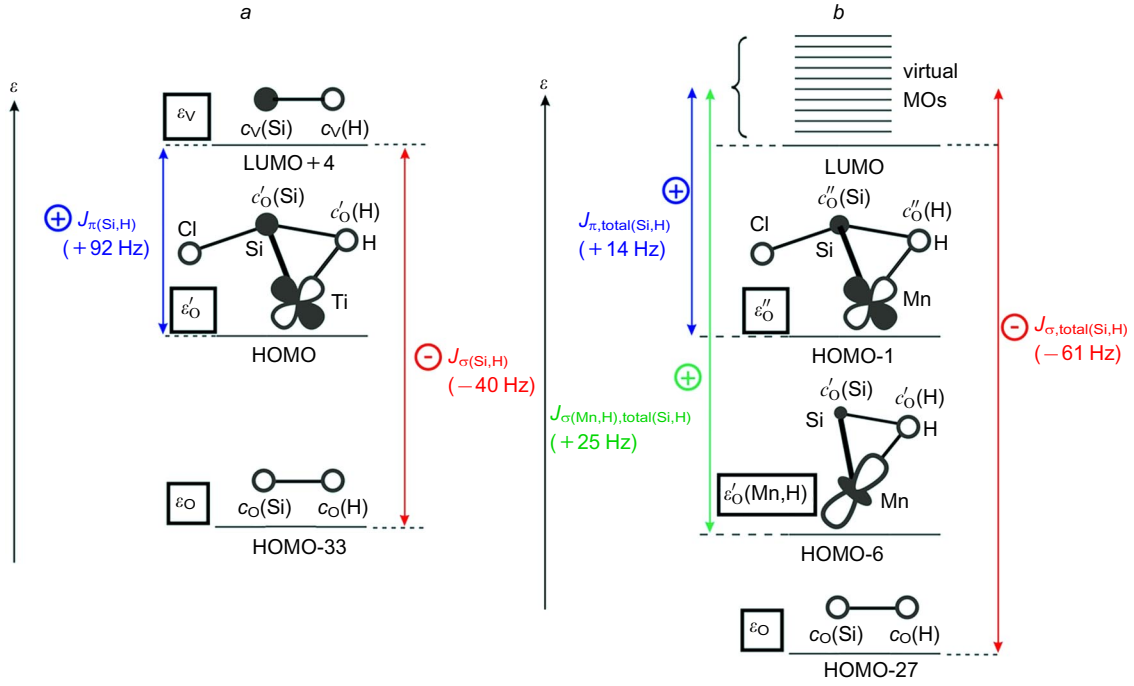


Figure 21. Decomposition of the $J_{Si,H}$ couplings of the silicon complexes into individual σ- and π-contributions from the pairs of interacting occupied and virtual MOs: (*a*) silicon – titanium complexes, (*b*) silicon – manganese complexes. In more detail, (*a*) the notation $J_{\sigma(Si,H)}$ denotes the mixing between the bonding σ(Si – H) and vacant σ*(Si – H) orbital which yields a negative contribution to the global $J_{Si,H}$ coupling. The mixing of the occupied HOMO (which is responsible for the M → L π back-donation) and the vacant σ*(Si – H) orbital (LUMO + 4) is labelled $J_{\pi(Si,H)}$ and provides a positive and dominant contribution to the Fermi contact term of $J_{Si,H}$. Note that only predominant orbital interactions of the Fermi contact terms are considered in this schematic drawing. (*b*) Decomposition of the $J_{Si,H}$ couplings of (Me)CpMn(CO)$_2$(HSiMe$_2$Cl) into individual $J_{\sigma,total(Si,H)}$ and $J_{\pi,total(Si,H)}$ contributions from pairs of interacting occupied and virtual MOs. The index total specifies that all interactions between all virtual orbitals and the respective occupied orbitals (HOMO-27, HOMO-6, and HOMO-1) are considered. The mixing of the occupied σ(Si – H) orbital (HOMO-27) with all vacant orbitals provides the dominating coupling contributions $J_{\sigma,total(Si,H)}$ to the negative Fermi contact term $J_{Si,H}$. For more details, see original publication. Reproduced from Meixner *et al.*[78] with the permission of the *American Chemical Society*.

bond angle did not provide a good measure of the extent of the oxidative addition in the whole series of **25**–**29**, since the metal-mediated Si—H bond-activation process was mainly controlled by the presence and extent of a local Lewis-acid site at the metal centre. Based on these results, it was concluded[77] that a positive sign of $J_{Si,H}$ in this series was due to the increase in the π-contributions to $J_{Si,H}$, which appeared from the increasing dominance of the Ti → σ* (H—Si—Cl) π-back-donation between the metal and the silane ligand, as the number of the electron-withdrawing ligands at the silicon atom increased. This trend appeared not to depend on the presence of the additional intramolecular interactions, which would be characterized by a pronounced σ(Ti—H)/σ*(Si—Cl) orbital interaction mechanism. According to the performed DFT studies, the latter interaction provided only a minor coupling contribution of less than 3 Hz to the total value of $J_{Si,H}$, which could be safely ignored.

In the next publication,[78] the authors extended their studies of the structural trends of $J_{Si,H}$ for the series of chromium, manganese, nickel, titanium, and iron complexes **18**–**24**. It was generalized that positive $J_{Si,H}$ were observed when M → L π-back-donation dominated (M stands for the transition metal, while L stands for the hydrosilane ligand). In contrast, negative $J_{Si,H}$ indicated the predominance of the significant covalent Si—H interactions. The decomposition of $J_{Si,H}$ couplings of the silicon–titanium and silicon–manganese complexes in terms of the individual σ- and π-contributions from the pairs of interacting occupied and virtual MOs, performed in this study, is schematically shown in Fig. 21. For more details, we direct the reader to the original publication.[78]

3.2. Spin–spin coupling constants $^{29}Si-^{13}C$

Early papers on the computation of this type of coupling constants were comprehensively reviewed by Blechta.[81] In a more recent time, the interest in this field has essentially diminished, however such papers do appear, as exemplified by a recent publication by Rusakova *et al.*,[82] where a computational study of the one-bond $^{29}Si—^{13}C$ spin–spin coupling constants has been performed at the SOPPA level in the series of sixty diverse silanes. A special attention in this paper was concentrated on the main accuracy factors, including the level of theory, the quality of the basis set, and the contribution of solvent and relativistic effects. To evaluate the role of the level of theory and a quality of a basis set on those calculations, three different theoretical levels of a general SOPPA scheme were examined, namely SOPPA(MP2), SOPPA(CC2), and SOPPA(CCSD), in combination with five augmented Dunning's basis sets — those from double to quintuple splitting quality, see Figs 22 and 23.

Based on the results of the performed study,[82] it was found that among three SOPPA-based methods tested in that study, SOPPA(MP2), SOPPA(CC2), and SOPPA(CCSD), the best result was achieved with SOPPA(CCSD), when used in combination with Sauer's basis set aug-cc-pVTZ-J. For the Dunning's basis sets, aug-cc-pVXZ (X = D, T, Q, 5), the decrease of MAE and MAPE started only from the quintuple-splitted aug-cc-pV5Z which implied that in the high-accuracy computations of $^{1}J_{Si,C}$ at the SOPPA level the aug-cc-pV5Z and higher Dunning's basis sets should be used. However, even more accurate results were achieved with a much cheaper triply-splitted Sauer's basis set aug-cc-pVTZ-J. The latter is of a triple zeta quality, but it includes four tight *s*-functions, being optimized for the correlated calculation of spin–spin coupling constants with a predominant Fermi contact term.

The combination of SOPPA(CCSD) with an aug-cc-pVTZ-J basis set was recommended as the most accurate and most effective computational scheme for the calculation of $^{1}J_{Si,C}$. The slightly less accurate, but essentially more economic SOPPA(MP2)/aug-cc-pVTZ-J and/or SOPPA(CC2)/aug-cc-pVTZ-J methods were recommended for the larger molecular systems. It was shown that solvent and relativistic corrections did not play a major role in the computation of the total values of $^{1}J_{Si,C}$. However, taking them into account noticeably improved agreement of calculation with experiment, so that taking them into consideration was strictly recommended in the high-accuracy calculations of $^{1}J_{Si,C}$. The rovibrational corrections were estimated as being, in average, of about 1 Hz or 1%–1.5% of the total value of $^{1}J_{Si,C}$.

In a more recent paper by Demissie,[83] fully relativistic four-component calculations of the one-bond and longer-range X—^{13}C (X = ^{29}Si, ^{73}Ge, ^{119}Sn, ^{207}Pb) spin–spin coupling constants were carried out in a series of silicon, germanium, tin, and lead alkynyl compounds in comparison with the two-component quasi-relativistic and non-relativistic results to reveal the meaning (contribution) of relativistic effects for these types of coupling constants. A correlation between calculated and experimental spin–spin coupling constants showed that the four-component relativistic DFT calculations with the PBE0 functional provided best results, as compared to their experimental values. A comparison of the two- and four-component relativistic methods for the calculation of these spin–spin coupling constants showed that scalar effects were dominant due to the relativistic increase in density and spin-density at the position of the nucleus, in agreement with the well-established trends.[84–90] It was thus concluded that for spin–spin couplings of these types (and for $^{n}J_{Si,C}$ in particular), the main relativistic effect was not due to the spin-orbit coupling but rather to the scalar relativistic contraction of *s*-shells. Overall, the inclusion of relativistic effects in the calculation of spin–spin coupling constants $^{n}J_{X,C}$ (X = ^{29}Si, ^{73}Ge, ^{119}Sn, ^{207}Pb) was very important for

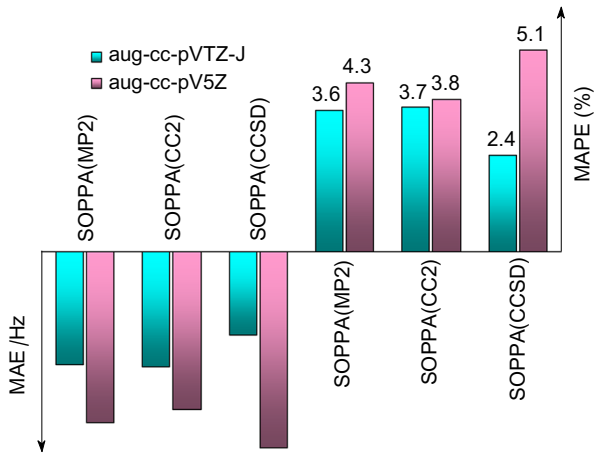


Figure 22. The diagram of MAE and MAPE of $^{1}J_{Si,C}$, calculated at the SOPPA(MP2), SOPPA(CC2), and SOPPA(CCSD) levels in a benchmark series of salient silanes. Reproduced from Rusakova *et al.*[82] with the permission of *John Wiley and Sons*.

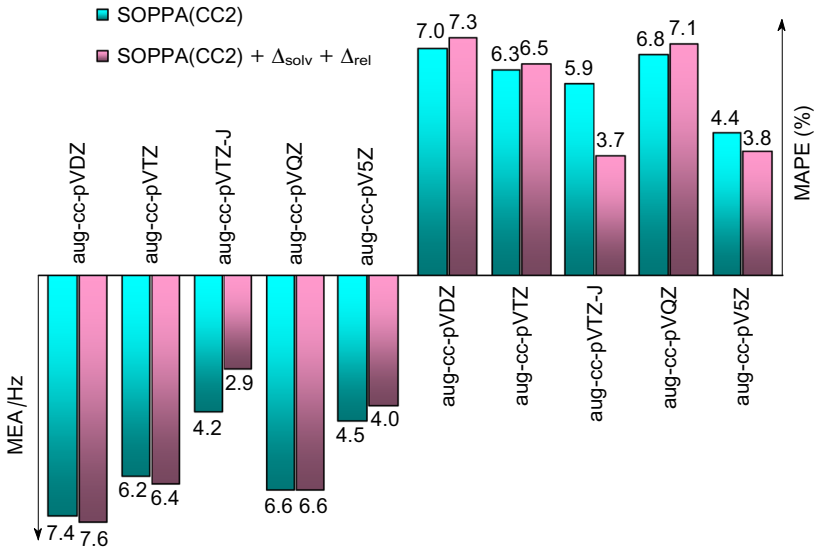


Figure 23. The diagram of MAE and MAPE of $^{1}J_{Si,C}$, calculated at the SOPPA(CC2) level in a benchmark series of salient silanes with different basis sets. Reproduced from Rusakova *et al.*[82] with the permission of *John Wiley and Sons*.

the qualitatively correct results since it depended on the behaviour of the wave function in a close vicinity to the coupled nuclei.

In the study performed by Demissie,[83] the spin – orbit contributions were calculated as the difference between the full four-component relativistic DFT calculations and the calculations with the removed spin – orbit effects, whereas the scalar relativistic contributions were calculated as differences between calculations with the removed spin – orbit effects and the non-relativistic results. The relativistic corrections were estimated as the difference between the full four-component relativistic and the non-relativistic values, all obtained using the PBE0 exchange-correlation functional and the dyall-cvtz basis set. For $^{n}J_{Si,C}$ couplings, the calculated values showed that the spin-orbit contributions to the coupling constants of all molecules were small, as compared to the scalar contributions. Overall, the scalar contributions were dominant over the spin – orbit contributions, which could be due to the low *s*-character of the corresponding Si – C bonds. Thus the net relativistic corrections in most of the molecules were shown to be negative, reducing the values of the corresponding $^{n}J_{Si,C}$ coupling constants. Even though the spin – orbit contributions were small, it was important to consider both the scalar and spin – orbit contributions in order to get accurate results.

A rather philosophical conclusion of that paper[83] was that 'the four-component relativistic method has reached a level of maturity that makes it a convenient and accurate tool to calculate indirect spin – spin coupling constants of large molecules involving heavy atoms' (and we will add here, based on the performed study, 'beginning with the fourth-row silicon').

In the most recent computational study by Jakubowska *et al.*,[91] the same set of compounds was investigated to calculate $^{n}J_{X,C}$ (X = ^{13}C, ^{29}Si, ^{73}Ge, ^{119}Sn, ^{207}Pb) by employing both coupled-cluster theory and DFT, the latter in the nonrelativistic domain and fully relativistic four-component version with different exchange-correlation functionals and basis sets. In addition, the property derivatives with respect to the molecular geometry parameters have been computed with the non-relativistic and relativistic Hamiltonians in order to evaluate the usefulness of calculated non-relativistic vibrational corrections. Generally, the coupled cluster method reproduced experimental values somewhat better than DFT. In the case of the latter, the performance of the B3LYP functional was most satisfactory. The relativistic effects became noticeable for the couplings involving tin and lead, and were next to negligible for silicon and, all the more so, for carbon. As an example, $^{1}J_{Si,C}$ and $^{2}J_{Si,C}$ calculated for ethynylsilane within fully relativistic and nonrelativistic approaches, differed by only about 1.5% – 2.5% of their total values.

3.3. Other coupling constants ^{29}Si – X

Computation of these rather exotic types of coupling constants received essentially much less attention than that for $^{n}J_{Si,H}$ and $^{n}J_{Si,C}$. The comprehensive overview of the calculation of ^{29}Si – X (X = ^{9}Be, ^{11}B, ^{13}C, ^{15}N, ^{29}Si, ^{31}P, and ^{77}Se), performed in the end of a previous and beginning of a current centuries, is presented in the early review by Wrackmeyer.[92] The salient values of these couplings are exemplified in Table 2, extracted from that review together with the calculated value of $^{1}J_{Si,F}$ taken from the paper[63] of approximately the same period of time.

As follows from these data, a relatively good agreement of B3LYP/6-311 + G(d,p) calculations with experiment for the coupling constants of silicon with the 'light' second-row elements (beryllium, boron, carbon, nitrogen, and fluorine) for compounds **30** – **34** is observed. However, a significant overestimation of calculated silicon couplings with 'heavier' third- and fourth-period elements (phosphorus, selenium) in compounds **36** and **37** is manifested, which is undoubtedly due to relativistic effects, not taken into account at this level. Unfortunately, no experimental value of $^{1}J_{Si,Si}$ for **35** is available to see how B3LYP/6-311 + G(d,p) calculations perform in this case with taking no relativistic effects at this level. It would be interesting to see whether relativistic effects would come into play (and to what extent) for silicon, but this could be done only provided the experimental value of this coupling constant is available.

Table 2. Representative one-bond spin–spin coupling constants of silicon with the isotopes of different elements, $^{1}J_{Si,X}$ (Hz), calculated at the B3LYP/6-311+G(d,p) level, as compared to experiment. Compiled from Wrackmeyer.[92]

Compound	Formula	X	Calc.	Exp.
30	$Me_3Si-BeCp$	^{9}Be	52.7	51.4
31	Me_3Si-BH_3	^{11}B	−69.5	−74.0
32	$SiMe_4$	^{13}C	−44.3	−50.8
33	$(H_3Si)_3N$	^{15}N	3.2	6.0
34	SiF_4	^{19}F	343.1 [a]	–
35	$Me_3Si-SiHMe_2$	^{29}Si	−6.3	–
36	$(Me_3Si)_3P$	^{31}P	84.8	27.2
37	$(Me_3Si)_2Se$	^{77}Se	143.1	109.8

[a] Calculated at the B3LYP/aug-cc-pVTZ level, taken from Ref. 63. Experimental values of spin–spin coupling constants of compounds **34** and **35** are not available.

One of the most representative examples, which finalizes this short section, is that reported by Cadars *et al.*,[93] who performed DFT calculations at the B3LYP/IGLO-III//IGLO-II level of geminal silicon-to-silicon spin–spin coupling constants across oxygen, $^{2}J_{Si-O-Si}$, of a model linear silicate dimer. Related calculations of the siliceous zeolite, shown in Fig. 24, whose framework is known to high accuracy from the single-crystal X-ray diffraction studies, yielded an excellent agreement between calculated and experimentally measured $^{2}J_{Si-O-Si}$ couplings. It was found that such calculations were extremely sensitive to the local framework structure, showing promise for the use of $^{2}J_{Si-O-Si}$ couplings to probe, establish, and refine the local structures of zeolites and layered silicates. Furthermore, this particular type of geminal couplings, $^{2}J_{Si-O-Si}$, being measured experimentally and/or calculated theoretically, were expected to have strong general potential for the use as the sensitive probes of molecularly ordered polymers, organic crystals, biomolecules, and inorganic or hybrid materials.

More examples of structural applications of rather exotic $^{29}Si-X$ couplings could be found in the above mentioned earlier review by Wrackmeyer.[92]

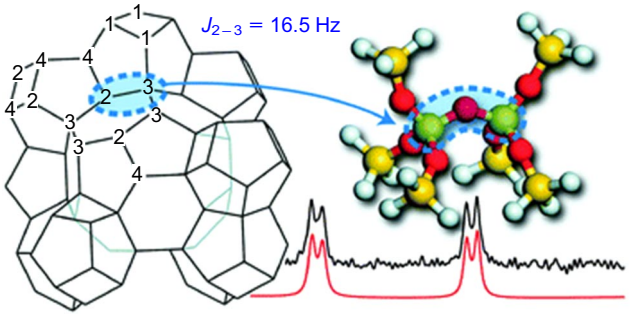


Figure 24. Schematic representation of the structure of siliceous zeolite, showing silicon atoms at the vertices of the polygonal shapes and oxygen atoms, bridging between adjacent silicon T-sites as straight lines. Shown on the right are experimental 1D slices (in black), extracted at the double-quantum frequencies and corresponding to different $^{29}Si-O-^{29}Si$ pairs of unequivalent silicon T-sites. The red solid lines are 1D spectral deconvolutions of the respective experimental slices, from which the $^{2}J_{Si-O-Si}$ scalar couplings have been obtained. Reproduced from Cadars *et al.*[93] with the permission of the *Royal Society of Chemistry*.

4. Conclusion

Calculations of ^{29}Si NMR chemical shifts and spin–spin coupling constants involving the ^{29}Si nuclei are rapidly progressing in modern chemical research. Nowadays, a number of DFT and *ab initio* approaches are widely used for this purpose. At the DFT level in the nonrelativistic domain, quasi-relativistic two-component approach, and fully relativistic four-component approximation, a variety of exchange-correlation functionals (PBE0, B3PW91, KT2, KT3, *etc.*) and basis sets from double to quintuple splitting quality (Dunning's aug-cc-pVXZ with X = D, T, Q and 5, Jensen's aug-pcS-n and aug-pcJ-n with $n = 1-4$, Sauer's aug-cc-pVTZ-J, relativistic Dyall's dyall.v3z, dyall.av3z, dyall.cv3z, and many others) are commonly used in such calculations. For spin–spin coupling constants treated at the non-empirical level, the most promising approaches in our practice are those based on Sauer's SOPPA(MP2), SOPPA(CC2), and SOPPA(CCSD) computational schemes.

Calculations of ^{29}Si NMR chemical shifts for silanes containing no 'heavy' elements (*i.e.* those beginning from the 4-th period) directly bonded to silicon could safely be performed at the non-relativistic level, since the contribution of 'neat' relativistic effects of silicon having no 'heavy' neighbours, are next to negligible. However, this situation dramatically changes when 'heavy' elements, beginning from the fourth period and neighbouring to the silicon atom, are present in the molecule. In this case, relativistic calculations at the two- and better four-component levels are strictly recommended. In addition, calculation of ^{29}Si NMR chemical shifts and spin–spin coupling constants involving the ^{29}Si nuclei are most likely to be performed with both the non-relativistic and relativistic Hamiltonians in order to evaluate the usefulness of relativistic effects and the non-relativistic vibrational corrections and medium effects.

Of major importance are the electronic and stereochemical effects, manifested in the ^{29}Si NMR parameters of organosilicon compounds, evaluated at different levels of theory with a special emphasis on their stereochemical applications. For ^{29}Si NMR chemical shifts, a good deal of interest is also focused on the less common solid state studies, in addition to more popular liquid state research. For spin–spin coupling constants, the main interest, covered in the present review, is concentrated on the most common $^{29}Si-^{1}H$ and $^{29}Si-^{13}C$ couplings.

References

1. S.P.A.Sauer. *Molecular Electromagnetism. A Computational Chemistry Approach*. (Oxford: University Press, 2012)
2. T.Helgaker, M.Jaszuński, K.Ruud. *Chem. Rev.*, **99**, 293 (1999)
3. T.Helgaker, M.Jaszuński, M.Pecul. *Prog. NMR Spectrosc.*, **53**, 249 (2008)
4. T.Helgaker, S.Coriani, P.Jørgensen, K.Kristensen, J.Olsen, K.Ruud. *Chem. Rev.*, **112**, 543 (2012)
5. D.Cremer, J.Grafenstein. *Phys. Chem. Chem. Phys.*, **9**, 2791 (2007)
6. J.Vaara. *Phys. Chem. Chem. Phys.*, **9**, 5399 (2007)
7. G.A.Aucar, R.H.Romero, A.F.Maldonado. *Int. Rev. Phys. Chem.*, **29**, 1 (2010)
8. M.Bühl, T.van Mourik. *WIREs Comput. Mol. Sci.*, **1**, 634 (2011)
9. *High Resolution NMR Spectroscopy: Understanding Molecules and their Electronic Structures*. (Ed. R.H.Contreras). (Amsterdam, The Netherlands: Elsevier, 2013)

10. Y.Y.Rusakov, L.B.Krivdin. *Russ. Chem. Rev*., **82**, 99 (2013)
11. F.A.A.Mulder, M.Filatov. *Chem. Soc. Rev*., **39**, 578 (2010)
12. L.B.Krivdin, R.H.Contreras. *Ann. Rep. NMR Spectrosc*., **61**, 133 (2007)
13. A.Navarro-Vázquez. *Magn. Reson. Chem*., **55**, 29 (2017)
14. Y.Xiao, W.Liu, J.Autschbach. *Relativistic Theories of NMR Shielding*, in: *Handbook of Relativistic Quantum Chemistry*. (Ed. W.Liu). (Berlin: Springer, 2017). P. 657
15. J.Autschbach. *Phyl. Trans. Royal Soc. A*, **372**, 1 (2014)
16. M.Repisky, S.Komorovsky, R.Bast, K.Ruud. In *Gas Phase NMR*. (Eds K.Jackowski, M.Jaszunski). (Cambridge: The Royal Society of Chemistry, 2016). P. 267
17. I.L.Rusakova, Y.Y.Rusakov, L.B.Krivdin. *Russ. Chem. Rev*., **85**, 356 (2016)
18. I.L.Rusakova, L.B.Krivdin. *Mendeleev Commun*., **28**, 1 (2018)
19. L.B.Krivdin. *Magn. Reson. Chem*., **57**, 897 (2019)
20. L.B.Krivdin. *Magn. Reson. Chem*., **58**, 5 (2020)
21. L.B.Krivdin. *Magn. Reson. Chem*., **58**, 15 (2020)
22. L.B.Krivdin. *Prog. NMR Spectrosc*., **105**, 54 (2018)
23. L.B.Krivdin. *Prog. NMR Spectrosc*., **108**, 17 (2018)
24. L.B.Krivdin. *Prog. NMR Spectrosc*., **112** – **113**, 103 (2019)
25. L.B.Krivdin. *Prog. NMR Spectrosc*., **102** – **103**, 98 (2017)
26. L.B.Krivdin. *Magn. Reson. Chem*., DOI: 10.1002/mrc.4965
27. L.B.Krivdin. *Magn. Reson. Chem*., DOI: 10.1002/mrc.4973
28. M.Milbradt, H.Marsmann, T.Heine, G.Seifert, T.Frauenheim. In *Organosilicon Chemistry V*. (Eds N.Auner, J.Weis). (Weinheim: Wiley-VCH, 2003). P. 324
29. M.Anafcheh, R.Ghafouri. *Phys. E*, **48**, 13 (2013)
30. O.V.Filonenko, V.S.Kuts, M.I.Terebinska, V.V.Lobanov. *Chem. Phys. Techn. Surf*., **6**, 263 (2015)
31. K.T.Butler, D.W.Lewis. *J. Phys. Chem. A*, **116**, 8786 (2012)
32. A.M.Rouf, H.Ottosson. *Molecules*, **17**, 369 (2012)
33. V.F.Sidorkin, E. F.Belogolova, V.A.Pestunovich. *Chem. – Eur. J*., **12**, 2021 (2006)
34. V.F.Sidorkin, E.P.Doronina, E.F.Belogolova. *Chem. – Eur. J*., **19**, 10302 (2013)
35. E.F.Belogolova, V.F.Sidorkin. *J.Phys. Chem. A*, **117**, 5365 (2013)
36. V.F.Sidorkin, E.F.Belogolova, E.P.Doronina. *Phys. Chem. Chem. Phys*., **17**, 26225 (2015)
37. E.P.Doronina, V.F.Sidorkin, N.F.Lazareva. *J.Phys. Chem. A*, **119**, 3663 (2015)
38. E.F.Belogolova, T.I.Vakul'skaya, V.F.Sidorkin. *Phys. Chem. Chem. Phys*., **17**, 12735 (2015)
39. V.F.Sidorkin, E.F.Belogolova, Y.Wang, V.Jouikov, E.P.Doronina. *Chem. – Eur. J*., **23**, 1910 (2017)
40. V.Romanovs, V.Sidorkin, E.Belogolova, V.Jouikov. *Dalton Trans*., **46**, 8849 (2017)
41. E.F.Belogolova, E.P.Doronina, V.F.Sidorkin. *Phys. Chem. Chem. Phys*., **20**, 26210 (2018)
42. E.F.Belogolova, G.Liu, E.P.Doronina, S.M.Ciborowski, V.F.Sidorkin, K.H.Bowen. *J.Phys. Chem. Lett*., **9**, 1284 (2018)
43. V.F.Sidorkin, V.A.Pestunovich, M.G.Voronkov. *Magn. Reson. Chem*., **23**, 491 (1985)
44. A.A.Nikolin, A.A.Korlyukov, E.P.Kramarova, D.E.Arkhipov, A.G.Shipov, Yu. I.Baukov, V.V.Negrebetsky. *Russ. Chem. Bull. Int. Ed*., **67**, 1299 (2018).
45. A.A.Korlyukov, D.E.Arkhipov, A.D.Volodin, V.V.Negrebetskii, A.A.Nikolin, E.P.Kramarova, A.G.Shipov, Yu.I.Baukov. *Russ. Chem. Bull. Int. Ed*., **68**, 137 (2019)
46. A.A.Korlyukov, Yu.V.Nelyubina. *Russ. Chem. Rev*., **88**, 677 (2019).
47. K.A.Chernyshev, L.B.Krivdin. *Russ. J.Org. Chem*., **48**, 1518 (2012)
48. K.A.Chernyshev, B.A.Gostevskii, A.I.Albanov, L.B.Krivdin. *Russ. J. Org. Chem*., **49**, 34 (2013)
49. K.A.Chernyshev, B.A.Gostevskii, L.B.Krivdin. *Russ. J. Org. Chem*., **49**, 832 (2013)
50. A.I.Poblador-Bahamonde, R.Poteau, C. Raynaud, O.Eisenstein. *Dalton Trans*., **40**, 11321 (2011)
51. C.Zhang, P.Patschinski, D.S.Stephenson, R.Panisch, J.H.Wender, M.C.Holthausen, H.Zipse. *Phys. Chem. Chem. Phys*., **16**, 16642 (2014)
52. S.V.Fedorov, Y.Y.Rusakov, L.B.Krivdin. *Russ. Chem. Bull. Int. Ed*., **64**, 551 (2015)
53. S.V.Fedorov, Y.Y.Rusakov, L.B.Krivdin. *J.Phys. Chem. A*, **119**, 5778 (2015)
54. S.V.Fedorov, Y.Y.Rusakov, L.B.Krivdin. *Russ. J. Org. Chem*., **53**, 643 (2017)
55. T.Charpentier, K.Okhotnikov, A.N.Novikov, L.Hennet, H.E.Fischer, D.R.Neuville, P.Florian. *J. Phys. Chem. B*, **122**, 9567 (2018)
56. A.Quintas, D.Caurant, O.Majérus, P.Loiseau, T.Charpentier, J.-L.Dussossoy. *J. Alloys Compd*., **714**, 47 (2017)
57. E.Gambuzzi, A.Pedone, M.C.Menziani, F.Angeli, D.Caurant, T.Charpentier. *Geochim. Cosmochim. Acta*, **125**, 170 (2014)
58. R.J.Evans, C.A.Fyfe, L.A.Groat, A.E.Lam. *Am. Mineral*., **97**, 329 (2012)
59. T.Charpentier, M.C.Menziani, A.Pedone. *Royal Soc. Chem. Adv*., **3**, 10550-10578 (2013)
60. A.Pedone. *Int. J. Quant. Chem*., **116**, 1520 (2016)
61. O.L.Malkina, D.R.Salahub, V.G.Malkin. *J. Chem. Phys*., **105**, 8793 (1996)
62. V.G.Malkin, O.L.Malkina, D.R.Salahub. *Chem. Phys. Lett*., **221**, 91 (1994)
63. W.Deng, J.R.Cheeseman, M.J.Frisch. *J. Chem. Theory Comput*., **2**, 1028 (2006)
64. E.A.Ebsworth, J.J.J.Turner. *Chem. Phys*., **36**, 2628 (1962)
65. E.V.R.de Castro, F.E.Jorge. *J. Chem. Phys*., **108**, 5225 (1998)
66. S.P.A.Sauer, W.T.Raynes. *J. Chem. Phys*., **113**, 3121 (2000)
67. S.P.A.Sauer, W.T.Raynes. *J. Chem. Phys*., **114**, 9193 (2001)
68. J.Ambati. Ph.D. Thesis. University of Kentucky (USA), 2011
69. J.Ambati, S.E.Rankin. *J. Phys. Chem. A*, **114**, 12613 (2010)
70. Y.Y.Rusakov, L.B.Krivdin, V.M.Nosova, A.V.Kisin. *Magn. Reson. Chem*., **50**, 278 (2012)
71. Y.Y.Rusakov, L.B.Krivdin, V.M.Nosova, A.V.Kisin, V.G.Lakhtin. *Magn. Reson. Chem*., **50**, 665 (2012)
72. Y.Y.Rusakov, L.B.Krivdin. *Magn. Reson. Chem*., **50**, 557 (2013)
73. Y.Y.Rusakov, L.B.Krivdin. *eMagRes*, **3**, 87 (2014)
74. S.J.Wilkens, W.M.Westler, J.L.Markley, F.Weinhold. *J. Am. Chem. Soc*., **123**, 12026 (2001)
75. J.E.Peralta, R.H.Contreras, J.P.Snyder. *Chem. Commun*., 2025 (2000)
76. F.Weinhold. Natural Bond Orbital Methods. In *Encyclopedia of Computational Chemistry*. Vol. 3. (Eds P.Schleyer, N.L.Allinger, T.Clark, J.Gasteiger, P.A.Kollman, H.F.Schaefer III, P.R.Schreiner). (Chichester, UK: Wiley, 1998). P. 1792
77. W.Scherer, P.Meixner, K.Batke, J.E.Barquera-Lozada, K.Ruhland, A.Fischer, G.Eickerling, K.Eichele. *Angew. Chem., Int. Ed*., **55**, 11673 (2016)
78. P.Meixner, K.Batke, A.Fischer, D.Schmitz, G.Eickerling, M.Kalter, K.Ruhland, K.Eichele, J.E.Barquera-Lozada, N.P.M.Casati, F.Montisci, P.Macchi, W.Scherer. *J. Phys. Chem. A*, **121**, 7219 (2017)
79. H.Li, L.C.Misal Castro, J.Zheng, T.Roinel, V.Dorcet, J.-B.Sortais, C.Darcel. *Angew. Chem., Int. Ed*., **52**, 8045 (2013)
80. W.Scherer, P.Meixner, J.E.Barquera-Lozada, C.Hauf, A.Obenhuber, A.Brück, D.J.Wolstenholme, K.Ruhland, D.Leusser, D.Stalke. *Angew. Chem., Int. Ed*., **52**, 6092 (2013)
81. V.Blechta. *Annu. Rep. NMR Spectrosc*., **67**, 97 (2009)
82. I.L.Rusakova, Y.Y.Rusakov, L.B.Krivdin. *Magn. Reson. Chem*., **52**, 413 (2014)
83. T.B.Demissie. *J. Chem. Phys*., **147**, 174301 (2017)

84. T.B.Demissie, M.Repisky, S.Komorovsky, J.Isaksson, J.Svendsen, H.Dodziuk, K.Ruud. *J. Phys. Org. Chem.*, **26**, 679 (2013)
85. T.B.Demissie, M.Jaszuński, E.Malkin, S.Komorovsky, K.Ruud. *Mol. Phys.*, **113**, 1576 (2015)
86. E.Malkin, S.Komorovsky, M.Repisky, T.B.Demissie, K.Ruud. *J. Phys. Chem. Lett.*, **4**, 459 (2013)
87. K.Ruud, T.B.Demissie, M.Jaszuński. *J. Chem. Phys.*, **140**, 194308 (2014)
88. S.Komorovsky, M.Repisky, O.L.Malkina, V.G.Malkin, I.Malkin Ondik, M.Kaupp. *J. Chem. Phys.*, **128**, 104101 (2008)
89. S.Komorovsky, M.Repisky, O.L.Malkina, V.G.Malkin. *J. Chem. Phys.*, **132**, 154101 (2010)
90. A.Wodyński, M.Repisky, M.Pecul. *J. Chem. Phys.*, **137**, 014311 (2012)
91. K.Jakubowska, M.Pecul, M.Jaszuński. *Theor. Chem. Acc.*, **137**, 41 (2018)
92. B.Wrackmeyer. *Annu. Rep. NMR Spectrosc.*, **57**, 1 (2006)
93. S.Cadars, D.H.Brouwer, B.F.Chmelka. *Phys. Chem. Chem. Phys.*, **11**, 1825 (2009)